



32 reviews the different types of unconfined PDCs, their deposits, dynamics and impacts, as well as the  
33 relationships between each element. Unconfined PDCs exist within a range of concentration, velocity  
34 and temperature: characteristics that are important in determining their impact. We define four end-  
35 member unconfined PDCs: 1. fast overspill flows, 2. slow overspill flows, 3. high-energy surges, and  
36 4. low-energy detached surges (LEDS), and review characteristics and incidents of each from  
37 historical eruptions. These four end-members were all observed within the 2010 eruptive sequence  
38 of Merapi, Indonesia. We use this well-studied eruption as a case study, in particular the villages of  
39 Bakalan, 13 km south, and Bronggang 14 km south of the volcano, which were impacted by slow  
40 overspill flows and LEDS, respectively. These two unconfined PDC types are the least described from  
41 previous eruptions, but during the Merapi eruption the overspill flow resulted in building destruction  
42 and the LEDS in significant loss of life. We discuss the dynamics and deposits of these unconfined  
43 PDCs, and the resultant impacts. We then use the lessons learned from the 2010 Merapi eruption to  
44 assess some of the impacts associated with the deadly 2018 Fuego, Guatemala eruption. Satellite  
45 imagery and media images supplementing fieldwork were used to determine the presence of both  
46 overspill flows and LEDS, which resulted in the loss of hundreds of lives and the destruction of  
47 hundreds of buildings in inundated areas within 9 km of the summit. By cataloguing unconfined PDC  
48 characteristics, dynamics and impacts, we aim to highlight the importance and value of accounting  
49 for such phenomena in emergency management and planning at active volcanoes.

50 **Keywords:** volcano, pyroclastic flow, pyroclastic surge, Merapi, Fuego

## 51 **1 Introduction**

52 Pyroclastic density currents (PDCs) are the deadliest volcanic hazard, accounting for nearly a third  
53 of all historical volcano-related fatalities (Brown et al. 2017). They are also some of the most complex  
54 and unpredictable volcanic phenomena, which makes accurate forecasting of their occurrence,  
55 characteristics and the area impacted difficult. In particular, the ability for PDCs to surmount  
56 topography and travel outside of river valleys can place them in direct contact with communities on  
57 the flanks of volcanoes. They can destroy whole towns and kill tens of thousands of people (e.g., St  
58 Pierre, Martinique, 1902; Lacroix, 1904) but little is known about their internal dynamic processes,  
59 and the ability to measure their dynamics in real time during eruptions does not yet exist. As a result,  
60 they pose a significant challenge for emergency management planning at explosive volcanoes in  
61 densely populated regions.

62 PDCs are gravity-driven mixtures of hot gases and fragmented particles (ranging from ash through  
63 lapilli to blocks and boulders). The term PDC encompasses a wide spectrum of densities and  
64 generation mechanisms, within which lie the two end-members of pyroclastic flow (dense, high  
65 particle concentration) and surge (dilute, low particle concentration) (Cole et al., 2015). A single PDC  
66 is commonly composed of two distinct layers - the denser, gravity driven basal “flow” layer and a  
67 more dilute, buoyant upper “surge” layer (Fisher 1995). While these layers can flow in unison under  
68 certain conditions (e.g., coupled PDCs in the 2015 eruption at Colima, Mexico; Pensa et al. 2019), it is  
69 common that they behave independently of each other, with the upper and lower layers moving at  
70 different speeds and having different characteristics (Breard and Lube 2017). The dense basal layer  
71 of a PDC (the flow) is topographically constrained so that their path typically remains confined to  
72 within a pre-existing channel, while the dilute, upper layer of PDCs (the surge) is less topographically  
73 constrained. Models of PDC transport regimes are improving in their sophistication, with the newest  
74 conceptual models including an intermediate flow layer between the dense basal and upper dilute  
75 layers (Lube et al., 2020). From a hazards perspective, this is extremely important, as it means the  
76 dilute, upper layer can detach from the lower, gravity driven flow, climbing topographic barriers and  
77 travelling to places that the rest of the PDC cannot (e.g., Nakada and Fujii 1993, Loughlin et al.  
78 2002a,b, Dufek et al. 2015, Jenkins et al. 2016). As a result, surges can unexpectedly inundate built  
79 areas outside of pre-existing channels, where people are present.

80 Here we present new detailed data connecting the geology and dynamics of the distal (>10 km) 5  
81 November 2010 unconfined PDCs at Merapi, focussing on their deposit characteristics, generation  
82 mechanisms and impacts to buildings, vegetation and victims, who were caught in the process of  
83 evacuating. We then use lessons drawn from the analysis of the Merapi 2010 eruption to assess PDC  
84 dynamics and impacts from the deadly June 2018 eruption of Volcán de Fuego in Guatemala. Using  
85 the same techniques as for Merapi 2010, we use satellite and media images to investigate loss of life  
86 and damage to structures caused by unconfined PDCs, supplemented by field studies focused on the  
87 deposits, and infer their types and dynamics. Data from both these eruptions provide an empirical  
88 foundation for better understanding and forecasting the impacts of unconfined PDCs on  
89 communities, highlighting the importance of accounting for the potential for such PDCs in emergency  
90 management planning, even where geological evidence of the PDCs is not preserved.

### 91 **1.1 Unconfined PDCs**

92 Several recorded volcanic tragedies in the past two centuries have resulted from surges that  
93 detached from their parent flows and inundated populated areas. While the upper more buoyant

94 surge layer is more likely to be unconfined by channel topography, and thus able to inundate a wider  
95 range of areas than the dense basal layer, dense flows can also become unconfined during their  
96 propagation. Such 'unconfining' of the flow and/or surge typically results from a change in the  
97 underlying syn-eruptive topography or by an increase of the local mass flux, volume or velocity of  
98 the dense flow, which can act to reduce channel capacity or redirect the flow away from the primary  
99 channel direction. These topographic changes can be natural or the result of human intervention, and  
100 there are broadly three topographic-related mechanisms that can caused a PDC to become  
101 unconfined:

- 102 1. *Lateral channel constriction*: narrowing of the channel in which a PDC is confined reduces the  
103 cross-sectional area available and may cause PDCs to expand vertically, making it easier for the  
104 PDC to escape the channel (e.g., Merapi 1994 and 2006). Such constrictions can be the result of  
105 natural topographic changes (through erosion and deposition) or concrete channel confinement  
106 for lahars (e.g., sabo dams);
- 107 2. *Vertical channel constriction*: shallowing of a channel or prior infilling by deposits will similarly  
108 have the effect of reducing the volumetric capacity of the channel and thus promoting the  
109 overspill of confined PDCs. Sediment retention dams intended to constrain the flow of lahars can  
110 promote this (e.g., Merapi 2010);
- 111 3. *Channel bends or obstructions*: Sudden changes in the direction of the confined flow path of a PDC  
112 can promote flow overspill or surge detachment, especially in combination with any of the above  
113 factors, as the PDC retains straight-line momentum (e.g., Soufrière Hills, June 1997);

114 PDC overspill and detachment are more likely when a channel is near capacity, for example through  
115 previous infilling from confined PDCs, which reduces the height difference between valley base and  
116 top (Lube et al., 2011, Charbonnier et al., 2013). This can be exacerbated by the pulsating behaviour  
117 of PDCs in some eruptions, in which flows from repeated pulses of eruption can progressively infill  
118 the channel (Sulpizio and Dellino, 2008). Unsteady flow conditions and increases in flow  
119 characteristics such as velocity, thickness, and volume may promote overspilling (Charbonnier et al.,  
120 2013). Unrelated to channel topography, a fourth mechanism can also cause flows and/or surges to  
121 be unconfined:

- 122 4. *Directed eruption*: Eruptions that begin from an explosive eruption that projects energy laterally,  
123 rather than as a result of dome or column collapse into channels, will often cause the ensuing  
124 PDCs to be unconfined from their point of inception (e.g., Mt. St. Helens 1980).

125 **1.2 PDC impacts**

126 The damage to communities caused by unconfined PDCs varies as a function of the PDC  
127 concentration, velocity, temperature, as well as other characteristics such as the transport of large  
128 clasts and debris that can act as missiles. For example, flow overspill typically causes impact through  
129 a combination of dynamic pressure, burial under metres of deposit, and/or thermal impact from  
130 temperatures that can reach over 800 °C (Cole et al., 2015), with near binary loss of life or  
131 infrastructure. By contrast, surge detachment can cause little physical damage because of low  
132 dynamic pressures and very thin (centimetres) remaining deposits, but their thermal impact can still  
133 cause casualties and indirect damage through fire (e.g., Baxter et al., 2005, Jenkins et al., 2013; Baxter  
134 et al., 2017). The dynamic characteristics of unconfined PDCs, and therefore the type and severity of  
135 impacts sustained, vary greatly depending on the generation mechanism and travel path of the PDC,  
136 as well as the mechanism through which overspill or detachment occurs. As a result, forecasting the  
137 occurrence and impacts associated with unconfined PDCs, across time and space, remains very  
138 challenging. Data for better understanding, and therefore forecasting, such events typically arise  
139 from field data, numerical modelling (e.g., Valentine and Wohletz, 1989, Neri et al., 2003, Esposti  
140 Ongaro et al., 2012, Benage et al., 2016) and/or large-scale experiments (e.g., Dellino et al., 2010,  
141 Lube et al., 2015, Brosch and Lube, 2020). Here, we focus on the value of the first: empirical  
142 observations and measurements, and how they can be supplemented with remote observations.

143 Despite their ability to cause serious impacts, unconfined PDCs have been previously described on a  
144 limited number of occasions, often tied to specific case studies in notable eruption sequences (e.g.,  
145 Soufrière Hills 1997). The lack of a broader comparative study of the different types of unconfined  
146 PDCs, and the relationships between their occurrence, deposits, dynamics and the impacts they  
147 cause, leaves a gap in the literature that we aim to fill with this study. We review the physical  
148 characteristics and devastating impacts associated with unconfined PDCs and provide new  
149 geological, impact and casualty data on a subset of these unconfined PDCs – slow overspill flows and  
150 low-energy detached surges during the Merapi 2010 eruption, Indonesia. We focus on these two  
151 types of unconfined PDC as their impacts are not necessarily binary, i.e. buildings, infrastructure and  
152 vegetation may be damaged but not destroyed, and probabilities of survival or escape may be higher  
153 than for the higher-energy flows and surges. Low-energy, detached surges have been well-  
154 documented in only two previous cases: the 1997 eruption of Soufrière Hills Volcano, Montserrat  
155 (Loughlin et al. 2002a, 2002b), and the 1994 eruption of Merapi, Indonesia (Abdurachman et al.  
156 2000; Voight et al., 2000). The Merapi 2010 eruption provides a particularly relevant case study as it

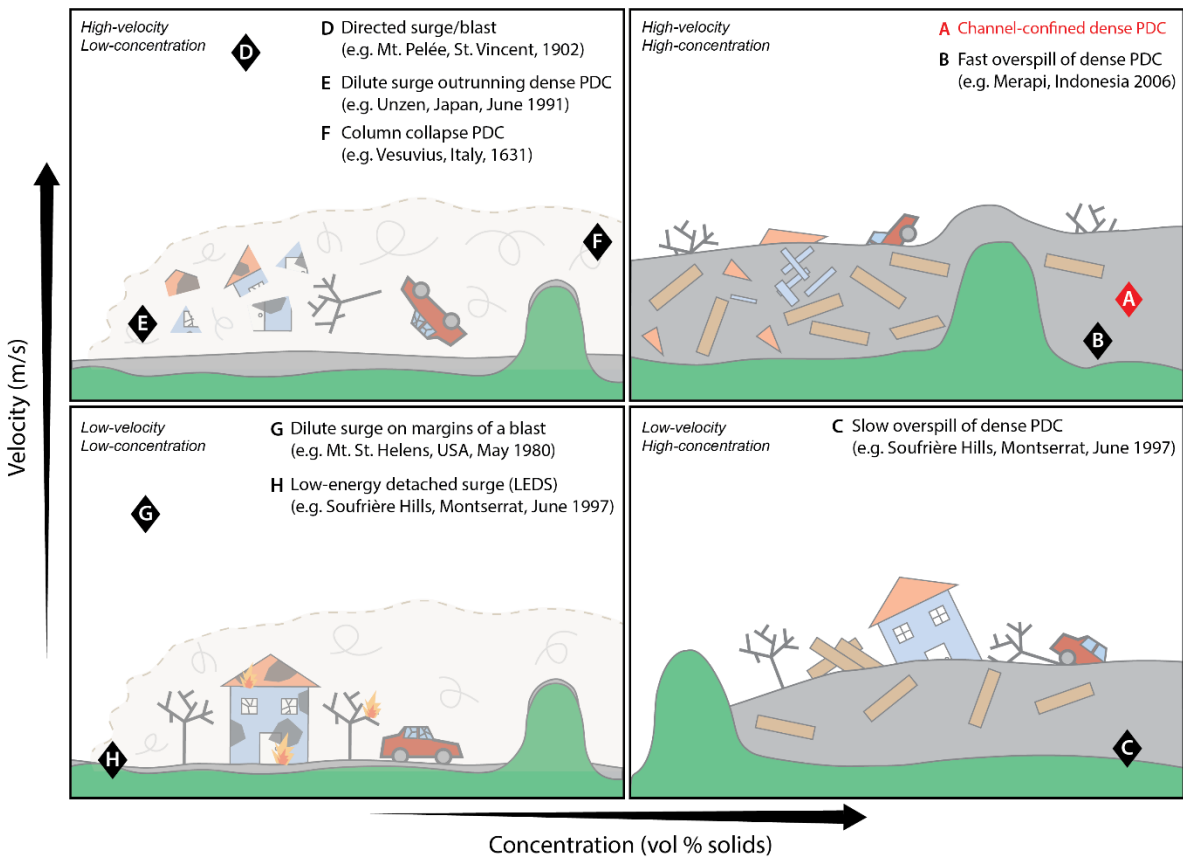
157 involved a wide variety of unconfined PDC types over the course of its eruptive sequence  
158 (Charbonnier et al., 2013, Cronin et al., 2013, Komorowski et al., 2013, Jenkins et al., 2016). This  
159 included significant impacts related to low-energy detached surges for which deposits were only  
160 centimetres thick and therefore unlikely to be preserved in the geological record. The events  
161 involving such detached surges and channel overflow flows during the 2010 Merapi eruption are  
162 summarised in Komorowski et al. (2013), Cronin et al. (2013), Charbonnier et al. (2013), Jenkins et  
163 al. (2013, 2016), and Baxter et al. (2017).

## 164 **2 Types of Unconfined PDCs**

165 Unconfined PDCs can be categorized by two main characteristics: their concentration and their  
166 velocity (Figure 1). The full spectrum of unconfined PDCs can be plotted within this matrix, with the  
167 following four end-member types as follows:

- 168 • **Fast overflow flows (high-velocity/high-concentration)** – spillover that occurs when a  
169 fast-moving, dense, channel-confined PDC is no longer constrained by a channel and invades  
170 adjacent areas;
- 171 • **Slow overflow flows (low-velocity/high-concentration)** – a dense, unconfined PDC that  
172 is moving at low speed, including the margin of a dense unconfined PDC that has slowed  
173 considerably from the speed of its confined parent flow;
- 174 • **High-energy surges (high-velocity/low-concentration)** – a dilute, directed PDC often  
175 stemming from a dome explosion that is typically unconfined from its inception;
- 176 • **Low-energy detached surges (low-velocity/low-concentration)** – the dilute, upper  
177 portion of a PDC that has decoupled from its denser basal parent flow, allowing it to travel  
178 to and invade areas not reached by the denser flows.

179 Characteristics associated with key types of unconfined PDCs are outlined in Figure 1, which  
180 highlights the wide range of impacts and deposits that can be produced; we provide more discussion  
181 and case studies below. Velocity and concentration thresholds are not easy to define but based on  
182 dynamics inferred or recorded in previous PDCs, we apply approximate thresholds of 5 m/s and 1%  
183 solid particle concentration by volume for the velocity and concentration, respectively, as indicative  
184 values for the boundary between “high” and “low” (Cole et al. 2015, Dufek et al. 2015) (Figure 1).



185

186 *Figure 1: Unconfined Pyroclastic Density Current (PDC) matrix with schematics showing the interaction*  
 187 *between PDC and topography, some impacts and an indication of the remaining deposit associated with*  
 188 *the four end-member unconfined PDCs. Black diamonds indicate the relative velocity and concentration*  
 189 *of the different types of unconfined PDCs, with one historical example shown for each type. The red*  
 190 *diamond represents the characteristics of a high-energy channel-confined PDC for comparison. Note:*  
 191 *Many of the eruptions provided as examples for each particular PDC type contained other PDC types as*  
 192 *well.*

193 **2.1 Fast overspill flows**

194 Fast overspill flows represent the high-velocity, high-concentration end-member of the unconfined  
 195 PDC matrix. These flows are closely related to their parent channel-confined PDCs, and typically  
 196 occur when the mass/volumetric flux of PDC in a channel surpasses the space available in the channel  
 197 to contain it; for example through channel infilling from previous deposits. The result is the flow  
 198 extending laterally beyond the banks of its confining channel and inundating areas adjacent to the  
 199 channel. This can also occur at bends in a channel where the straight-line momentum of the PDC is  
 200 sufficient to overtop the topographic margins of the channel. As a result, overspill flows are typically  
 201 close to the velocity of their parent channel-confined flows, which typically travel at speeds of up to  
 202 30 m/s and occasionally up to 60 m/s (Cole et al. 2015).

203 Overspill PDCs maintain both their high temperature and dynamic pressure, and thus cause damage  
204 through both heat and force. Parent channel-confined flows from hot lava dome collapse can be over  
205 600 °C, and fast overspills have been determined in several occurrences to have temperatures at or  
206 near their parent flows (e.g., Trolese et al. 2018, Wibowo et al. 2018), which can have dynamic  
207 pressures over 100 kPa near source and over 15 kPa in distal areas (Macorps et al. 2018). As with  
208 channel-confined PDCs, overspill flows typically destroy everything in their path, and cause the death  
209 and burial of people in inundated areas. For example, overspill flows during the 2006 eruption of  
210 Merapi caused two deaths through burial, and destroyed several buildings in the village of Kaliadem,  
211 ~5 km from the volcano (Gertisser et al. 2012). Similar impacts are sustained by vegetation and  
212 infrastructure, with the high dynamic pressures damaging, bending, or completely knocking down  
213 trees and utility poles (e.g., Soufrière Hills June 1997, Loughlin et al. 2002; Merapi 1994;  
214 Abdurachman et al. 2000).

215 Since these overspill flows represent only the portion of the flow capable of extending beyond the  
216 channel, the deposits can be thin relative to the channel-confined PDC, but still geologically  
217 significant, on the order of 10s of centimetres to metres thick. Overspill deposits in the 2010 Merapi  
218 eruption were typically ~1-2 m thick, and in isolated locations up to 5 m thick (Cronin et al., 2013),  
219 significantly thinner than the metres-thick channelized deposits, but thicker than the centimetres  
220 thick surge deposits (Charbonnier et al. 2013, Komorowski et al. 2013). Fast overspill flow deposits  
221 are typically poorly sorted and can contain up to metre-sized blocks in a medium or fine-grained ash  
222 matrix and are often not significantly visually distinct from confined flow deposits other than a  
223 generally lower presence of large clasts (Charbonnier and Gertisser 2008, Gertisser et al. 2012).

## 224 **2.2 *Slow overspill flows***

225 Low-velocity, high-concentration PDCs are frequently represented by the peripheral edges or front  
226 of a slowing flow, but can also happen when a slow-moving dense flow escapes the bounds of its  
227 channel. As flows (channel-confined or not) reach areas more distal from the volcano or branches of  
228 the flow move farther from the primary flow axis, they reduce in energy (and therefore velocity) as  
229 a result of basal drag or friction acting on the dense layer while maintaining the same concentration  
230 (Shimizu et al. 2019). The result is a slow moving, but still highly-concentrated PDC. These dense  
231 slow-moving flows are easily stopped by topographic barriers (e.g., Soufrière Hills, Loughlin et al.  
232 2002a,b), which the less dense surge portions of the PDC are capable of decoupling from and  
233 surpassing. The fronts of slowing flows can have velocities that have dropped to 1-2 m/s (Cole et al.  
234 2015).

235 The high-concentration and typically high temperatures (similar to or slightly cooler than their  
236 parent fast overspill flows, Trolese et al. 2018) of these flows means that they are still mostly fatal  
237 for victims caught within their path; however, impacts on the built environment can be less binary.  
238 The lower energy and dynamic pressures associated with a slower moving flow leads to inundation  
239 or damage of buildings and other infrastructure, with the peripheral parts of flows sometimes  
240 moving into or around impacted structures rather than sweeping them away (as described in Section  
241 3.3). Nevertheless, a building that has been inundated with PDC deposits, but is largely undamaged,  
242 remains uninhabitable for its owner. Damage to trees and other vegetation is typically a function of  
243 the temperature and thickness of deposits, i.e. burial, rather than the violent total or partial  
244 blowdown or complete removal associated with higher dynamic pressures. As in fast overspill  
245 deposits, the concentrated nature of the flow results in a geologically significant poorly sorted  
246 deposit up to several metres (e.g., deposits from the 2006 eruption of Merapi were up to 8 m thick;  
247 Gertisser et al. 2012), although deposits become thinner (10s of centimetres or more) than the  
248 channel-confined parent flow the farther from the parent flow they are found (Charbonnier and  
249 Gertisser, 2008). The deposits are generally texturally and compositionally nearly identical to fast  
250 overspill deposits, and as a result the speed of an overspill flow is difficult to determine from deposit  
251 characteristics alone — in these cases, impacted infrastructure, as well as the extent of a singed zone  
252 from the overbank deposits, can be helpful for determining flow velocity (Charbonnier and Gertisser  
253 2008).

### 254 **2.3 High-energy surge**

255 High-velocity, low-concentration PDCs are classified as high-energy surges, most commonly  
256 represented by directed blast eruptions, column collapse PDCs, and high-energy detached surges that  
257 decoupled from their parent PDCs. Directed blasts typically spread laterally from their source (most  
258 often the summit of a volcano) and are frequently generated by the explosion of a summit lava dome,  
259 shallow plug, or cryptodome, or through edifice collapse. These directed blasts are unconfined PDCs  
260 from point of origin, and tend to cover a very wide range, relatively unaffected by topography or  
261 channel confinement. Column collapse PDCs form from the gravitational collapse of a sustained ash  
262 column, and in many cases are characteristically similar to blast eruptions (e.g., Mt. Lamington, Papua  
263 New Guinea 1951; Belousov et al., 2020). By contrast, high-energy detached surges may originally be  
264 coupled with a fast-moving dense component and become unconfined by escaping the channel or  
265 otherwise changing direction from their parent flows, while maintaining their high velocities and  
266 dynamic pressures. Near source, velocities of directed blasts may be as high as 150 m/s (e.g., Mt. St.

267 Helens 1980) and typically over 90 m/s (Cole et al. 2015), while high energy detached surges  
268 maintain speeds up to those of their parent PDCs (up to ~60 m/s; Yamamoto et al. 1993).

269 Directed blasts frequently have high dynamic pressure (over 10 kPa) close to source and along the  
270 primary flow axis, but lower dynamic pressures (less than 1 kPa) in more distal areas (e.g., Jenkins  
271 et al., 2013, Gueugneau et al. 2020) and in measured cases have shown temperatures over 300 °C  
272 (Cole et al. 2015). This results in a wide range of effects on humans, the built and natural  
273 environment, with fatalities and destruction from blunt trauma and thermal impacts in proximal  
274 zones, and with injuries and relatively little damage in the peripheral zones. In well documented  
275 cases such as the 1631 eruption of Vesuvius, column collapse PDCs displayed many directed blast  
276 characteristics, causing near total damage in the most affected areas through high dynamic-pressure  
277 and covering a widespread area (Rosi et al., 1993). Similar to blasts, the intensity of these PDCs wanes  
278 on the margins, where they can display non-binary impacts, with survival of people and structures  
279 indicating characteristics consistent with slow margins of dense PDCs as well as low-energy, dilute  
280 surges (Rosi et al., 1993). For example, the 1902 column collapse from La Soufrière, St Vincent,  
281 showed extensive damage in areas near source (Anderson and Flett 1903, Baxter 1990), but was not  
282 capable of overturning trees or sturdy structures by the time it reached heavily inhabited areas, ~8  
283 km from source (Baxter 1990). Despite this, there were over 1500 deaths as well as nearly 200  
284 hospitalizations (with 80 subsequent deaths) largely from burns and the asphyxiating effects of the  
285 ash (Will 1903, Baxter 1990). Similarly, in the 1902 Mount Pelée blast eruption (which had a death  
286 toll of ca. 29,000), people in St Pierre, ~8 km from source, were severely burned by PDCs and fires  
287 with many laying prone in the “pugilistic attitude” frequently associated with deaths due to  
288 temperatures over 200 °C (Anderson and Flett 1903, Will 1903, Lacroix 1904, Baxter 1990).

289 Detached pyroclastic surges that decouple from and/or outrun their parent flows can also maintain  
290 high dynamic pressure despite their low concentration. These surges are more capable of  
291 overcoming topographic barriers than their parent dense PDC, as was the case in the deadly June  
292 1991 Unzen eruption, in which dilute surges detached from their parent flows and outran them by  
293 0.8 km, unexpectedly reaching an inhabited area where 43 people were killed (Nakada and Fujii  
294 1993). The dynamic pressures of these surges were high enough (up to 8 kPa in some parts of the  
295 surges; Clarke and Voight 2000) to destroy 50 houses, flatten trees, and move cars tens of metres  
296 (Nakada and Fujii 1993, Cooper 2018). Similarly, some high-energy detached surges in the 1994  
297 Merapi eruption maintained dynamic pressures that remained high enough to topple masonry walls,

298 down trees, strip roof tiles, and destroy bamboo huts 5 km from source (Abdurachman et al. 2000),  
299 which we estimate requires dynamic pressures of at least 2 kPa.

300 Deposits from these dilute, but high energy, surges are generally quite thin, but can reach greater  
301 thicknesses in depressions and valleys. Following the Unzen eruption, surge deposits were typically  
302 no more than 20 cm thick (Nakada and Fujii 1993) and were sometimes only a few centimetres thick,  
303 in contrast to the up to 10 m thick deposits from the parent flows (Miyahara et al. 1992). Deposits in  
304 the 1902 Mt. Pelée blast are estimated to range from 1.5 m along the main flow axis to 30 cm at the  
305 margins (Hovey 1904, Bourdier et al. 1989). Deposits from the 26 December 1997 blast at Soufrière  
306 Hills ranged from a few cm to 3 m outside of channels, while deposits were up to several metres thick  
307 in river valleys (Belousov et al. 2007). High energy blasts often leave a distinctive two-layer deposit  
308 (e.g., Soufrière Hills 1997, Merapi 2010) consisting of a basal, poorly-sorted, coarse layer that  
309 typically includes ripped up clasts of the underlying surface, overlain by a much finer-grained, better  
310 sorted deposit with some internal bedding (Brown and Andrews 2015; Komorowski et al., 2013).

#### 311 **2.4 Low-energy detached surge (LEDS)**

312 LEDS represent the low-velocity, low-concentration end of the unconfined PDC spectrum. These  
313 slow-moving surges (~1-2 m/s) represent the upper dilute layer of a PDC that has detached from its  
314 dense, basal flow layer (Lube et al 2011, Cole et al. 2015, Dufek et al. 2015). The buoyant nature of  
315 these surges allows them to easily overcome topographic barriers. In recorded events, these surges  
316 are most commonly seen moving laterally from their confined parent flows and escaping channels,  
317 leading to unexpected inundation of inhabited areas. How, why or where along the flow path a surge  
318 detaches is typically related to a change in the underlying syn-eruptive topography and/or the  
319 pulsative nature of the eruption, which can act to reduce channel capacity or redirect the channel  
320 away from the straight-line flow inertia, as described in the Introduction.

321 Due to their low velocity and concentration, and thus low dynamic pressure (typically <2 kPa), LEDS  
322 damage to buildings, infrastructure or vegetation is typically minor (with the exception of secondary  
323 damage through fire). For example, in the June 1997 Soufrière Hills eruption, LEDS were not capable  
324 of blowing down trees or poles at distances greater than 2 km from source (Cole et al. 2002) and  
325 damage to buildings was caused almost exclusively by temperatures up to around 400 °C (Baxter et  
326 al. 2005). The impact for humans can range from minor through to fatal burns injuries, with the  
327 chances of survival influenced by the LEDS temperature and duration as well as how much skin is  
328 exposed by clothing, to what extent the victims breathe in the LEDS, and the availability and timing

329 of medical resources (Baxter, 1990). The bodies of victims in such PDCs often show evidence of brief  
330 exposure to extreme heat, with many of the limbs flexed into the “pugilistic attitude” associated with  
331 fire and PDC deaths (e.g., Soufrière Hills, June 1997, Merapi 1994: Baxter, 1990; Baxter and Horwell,  
332 2015; Baxter et al., 2017).

333 Temperatures in these types of surges have been observed to be at least 180 °C and up to over 410  
334 °C based on both direct measurements (Soufrière Hills 1997; Loughlin et al. 2002a) and proxy  
335 estimates based on damage to vegetation and buildings (Merapi; Voight and Davis 2000, Unzen; Fujii  
336 and Nakada 1999). In some events a “sear zone” or “singe zone” of charred vegetation was seen to  
337 extend up to 25 m beyond the distal margins of surge deposits (Loughlin et al. 2002a).

338 The deposits of LEDCs are characterized by their relative thinness and poor preservation in the long-  
339 term geologic record. In most historical cases, these surges have been recorded as thin as a few  
340 centimetres and no thicker than 20 cm, even when associated with metres-thick, channel-confined  
341 PDCs (e.g., Soufrière Hills 1997; Cole et al. 2002, Druitt et al. 2002; Merapi 1994; Abdurachman et al.  
342 2000; Unzen 1991; Miyahara et al. 1992). Deposits tend to mantle the landscape as a result of settling  
343 from the dilute surge (Druitt et al. 2002) and are typically thinnest in open areas (Abdurachman et  
344 al. 2000). Most observed deposits are massive and normally graded, generally lacking any internal  
345 stratification, but deposits may contain multiple discrete layers if the event involved more than one  
346 surge pulse (Abdurachman et al. 2000, Cole et al. 2002, Druitt et al. 2002). In most cases, the deposits  
347 are poorly sorted ash but may contain lapilli and rare blocks in addition to gas segregation pipes and  
348 mixed in soil and charred wood fragments picked up in transit (Abdurachman et al. 2000, Druitt et  
349 al. 2002).

350 Single eruptive events may contain both high- and low-energy detached surges, as seen in the 1991  
351 Unzen eruption. In the June event, deadly high-energy surges killed 43 people and had dynamic  
352 pressures large enough to sweep away cars and trees in one area (Cooper 2018), while low-energy  
353 surges were capable of burning, but not bending or breaking, trees in other areas (Nakada and Fujii  
354 1993). Similarly, in the September Unzen event, high-energy surges in some locations were powerful  
355 enough to sweep away cars and trees damaged in the earlier eruption, while in another location low-  
356 energy surges caused damage only through heat, melting vinyl and charring building windows on the  
357 volcano-facing side of the buildings (Fujii and Nakada 1999). Dynamic pressures in these events may  
358 be up to 8 kPa in the high-energy surges, and lower than 2 kPa in the low-energy surges (Clark and  
359 Voight 2000).

### 360 **3 The 2010 Merapi eruption**

361 The full spectrum of confined and unconfined PDCs can occur within one eruption, affecting multiple  
362 places at the same time, or the same place at multiple different times. PDCs produced during the 2010  
363 eruption of Merapi in Indonesia provided one such example. Post-eruption field studies of the PDC  
364 impacted areas offered a unique opportunity to characterise the range of PDC types, their dynamics,  
365 deposits and interaction with populated areas to the south of the volcano. Here, we synthesise the  
366 sequence of PDC events and their impacts and present new data for key villages along the Gendol  
367 river. We focus on slow overspill flows and low-energy detached surges, as these two unconfined  
368 PDC end-members and their impacts are poorly documented in the literature.

369 After approximately one year of unrest, Merapi volcano began a new eruptive sequence on 26  
370 October 2010 with the explosion of a cryptodome and associated high-energy PDCs laterally directed  
371 towards the south. These initial PDCs extended 6.8 km from the summit and killed 35 people who  
372 had not evacuated (Jenkins et al., 2013, 2016). Unusually rapid dome growth (to 25 m<sup>3</sup>/s), with  
373 recurrent explosions and PDCs continued from 29 October until the paroxysm on 5 November  
374 (Surono et al. 2012, Pallister et al. 2013, Komorowski et al., 2013, Charbonnier et al., 2013). On 5  
375 November, starting at 00:02 local time (UTC +7), a series of five laterally directed dome explosions  
376 occurred, concurrent with retrogressive collapse of the dome, resulting in at least four distinct types  
377 of PDC in under 15 minutes: high-energy unconfined PDCs, dense valley-confined flows, overspill  
378 flows, and detached surges (Komorowski et al. 2013). Further gravitational dome collapse, fountain  
379 and sub-Plinian column collapse led to PDCs that extended to 15.5 km in the Gendol valley in the  
380 south, with flow overspills and low-energy detached surges extending 700 m from the channel and  
381 up to 200 m from the parent flow (Charbonnier et al. 2013, Komorowski et al. 2013, Jenkins, et al.,  
382 2016). PDC overspill and detachment along the more distal parts of the Gendol channel (>8 km from  
383 source) during this paroxysmal phase killed ~170 people (Jenkins et al., 2013, 2016) and damaged  
384 (n=395), severely damaged (removed the roof: n=108) or destroyed (n=645) 1,148 buildings. This  
385 event was termed a 'centennial' eruption (Surono et al., 2012), as this magnitude and style of eruption  
386 is seen approximately every 100 years at Merapi.

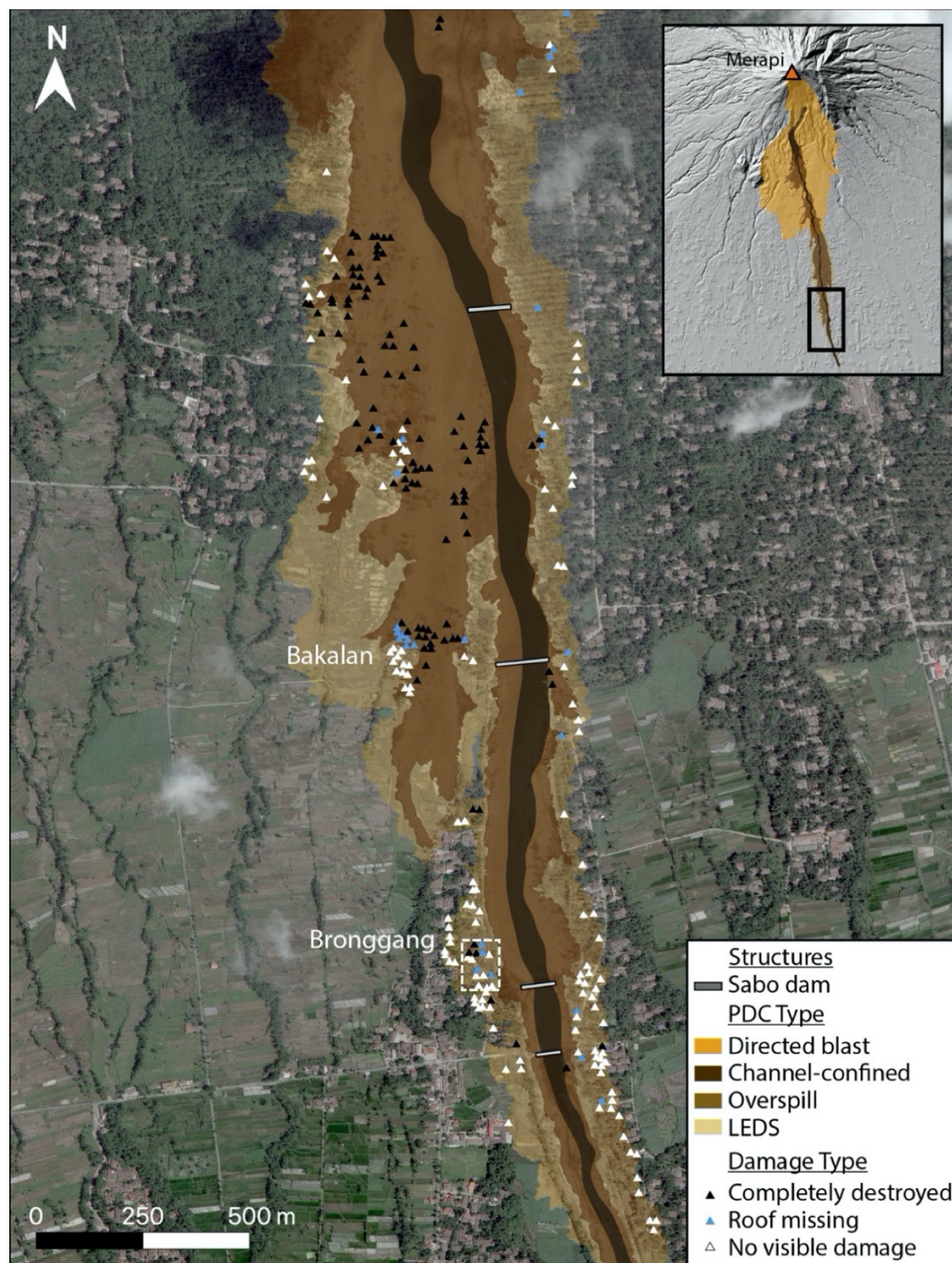
387 Field visits to the Merapi area three weeks after the 5 November 2010 event, and several times over  
388 the years that followed, allowed some of the authors [SF], SJC, JCK, and PJB] to collect detailed field  
389 data on confined and unconfined PDCs produced during the eruption. The geology, dynamics and  
390 impacts associated with the directed blast that affected a large swathe of the upper flanks to ~8 km

391 from the summit are presented in Komorowski et al. (2013) and Jenkins et al. (2013). Here, we focus  
392 on the generation mechanisms, deposits, impacts and inferred dynamics associated with i) slow  
393 overspill flows, and ii) low energy detached surges in villages along the Gendol river channel more  
394 than 10 km to the south of the summit. Fast overspill flows were also observed along the Gendol, but  
395 impacts were total, with all buildings, vegetations and victims buried with no observable remains.  
396 Uniquely, our field studies combined geological and engineering expertise in collecting and  
397 interpreting data on the deposits and physical impacts of the unconfined PDCs, which could be cross-  
398 referenced with medical data on the nature of burns injuries to victims. Some of the geology  
399 (Charbonnier et al., 2013, Cronin et al. 2013) and impacts (Jenkins et al., 2013; 2016; Baxter et al.,  
400 2017) from these more distal unconfined PDCs during the Merapi 2010 eruption have been discussed  
401 previously; here we present data not included in these studies. We hope that these data and  
402 interpretations are valuable for emergency management planning in providing the first multi-  
403 disciplinary case study of unconfined PDCs and their impacts.

### 404 **3.1 Case study sites**

405 We focus on two distinct type of unconfined PDC, for which we discuss the associated generation  
406 mechanisms, dynamics, impacts and deposits at two villages (Figure 2):

- 407 • Bakalan, 12.6 km straight-line distance from the summit and on the western edge of the Gendol  
408 river channel. The distal slow-moving portion of a fast overspill flow on 5 November inundated  
409 31 buildings within this village, with associated LEDS impacting a further 9; we concentrate on  
410 the impacts within the area inundated by the dense flow for this case study. Residents had  
411 evacuated the village prior to flow inundation.
- 412 • Bronggang village, ~13.5 km from the summit, on the western edge of the Gendol river channel,  
413 and bordering a sabo dam bridge that crosses the channel. During the 5 November paroxysmal  
414 phase of the eruption, LEDS impacted 48 buildings in Bronggang, killing 54 people who were in  
415 the process of evacuating.



416

417 *Figure 2: Channel-confined, overspill and detached PDCs along the Gendol river valley following the 5*  
 418 *November 2010 eruption of Merapi. Coloured triangles indicate level of damage observed in buildings*  
 419 *in pre- and post-eruption satellite images (Jenkins et al., 2013). Digital Globe optical Basemap imagery*  
 420 *(image acquired 11 Nov, 2010). White box surrounding buildings in Bronggang shows the locations of*  
 421 *buildings presented in Figure 5. Inset shows the village locations relative to the summit and wider PDC*  
 422 *impacted area.*

## 423 **3.2 Slow overflow flow: Bakalan village**

### 424 3.2.1 Generation

425 The flow first overflowed the main Gendol channel nearly 2 km upstream to the north, likely because  
426 of a bend in the channel towards the east and previous infilling of the channel with PDC deposits  
427 emplaced on 4 and 5 November (Charbonnier et al., 2013). Significant narrowing of the channel, and  
428 thus a reduction in channel capacity, approximately 1 km to the north upstream of Bakalan village,  
429 along with a number of sabo constrictions along the channel, may also have played a role in creating  
430 further overflow flows that inundated the village (Figure 2). Bakalan marks the distal margin of the  
431 overflowing flow, with 9 of the 40 buildings in the village affected by LEDS, and 31 by the overflowing  
432 flow (Figure 2).

### 433 3.2.2 Impacts

434 Slow overflow flows up to 2 m thick inundated 6 buildings without destroying, burying or sweeping  
435 them away (Figure 3a-c); a further 8 sustained major damage to the roof and some walls but  
436 remained partially standing (Figure 3d). Less resistant timber outhouses and animal shelters were  
437 destroyed by any inundation of dense flow. The gradation of building damage from complete  
438 destruction through to buildings remaining standing, despite flow having inundated the building  
439 envelope, was gradual but extended over a relatively short distance of ~50 m. Within this zone of  
440 rapid damage attenuation, building conditions fell mostly into one of two categories (with increasing  
441 distance from the parent flow):

- 442 1. Inundation with little to no structural damage, although roof tiles, rafters and purlins were lifted  
443 from the overhanging portion of the roof facing the flow. Roof tiles were cracked and/or  
444 penetrated by larger clasts carried within the dilute component of the PDC (Figure 3a and b).
- 445 2. Dense flow blocked by the walls of buildings, with little to no inundation through openings such  
446 as cracked glazing or doors; roof tiles remained unaffected (Figure 3c).

447 In addition to these main scenarios, we observed more severe damage where: i) isolated fires had  
448 ignited building contents and burned roof supports causing roof failure in one or more rooms, and ii)  
449 boulders of up to 1 m diameter carried within the flow caused structural failure of one or more walls  
450 (Figure 3d). Buildings in Bakalan village that were outside of the dense flow overflow and affected  
451 only by LEDS sustained similar impacts to those in the Bronggang area (Section 3.3). It is possible  
452 that fires observed in the area inundated by the dense flow were ignited by the passing of LEDS that

453 preceded the dense overspill, particularly as fire damage is observed in those buildings in Bakalan  
454 that were impacted only by the LEDS. However, any damage caused by the LEDS is expected to be of  
455 lesser consequence than that caused by the dense overspill; the brief gap in time between the two  
456 PDCs means that the temperature of the LEDS and flows were likely not markedly different, i.e. fires  
457 apparently caused by LEDS could also have been caused by the flow.

458 People were evacuated from Bakalan prior to the 5 November event, although locals reported  
459 between four and five fatalities in the village.



460  
461 *Figure 3: Photos of slow overspill flow impacts in Bakalan village including: a) Thick deposits of up to*  
462 *2.5 m partially burying houses and causing structural damage on upflow side of structure, b) inundation*  
463 *with minor structural damage, c) flows blocked by building fronts, resulting in little to no inundation,*  
464 *d) severe structural damage caused by large boulders carried by the dense flow. Photos taken 7*  
465 *December 2010 by S.F. Jenkins.*

### 466 3.2.3 Deposits

467 Stratigraphic sections studied after one rainy season in the Bakalan village show a massive, poorly-  
468 sorted overspill flow unit with blocks inside an ash-rich matrix, of ~2-3 m thickness overlying three

469 1-8 cm thick LEDS units at the base. Overbank deposit thicknesses in the Bakalan area vary from 2 to  
470 7 m and two overbank units are present in stratigraphic sections located at the overspill point, ~1 km  
471 upstream of the village (Figure 2). Based on stratigraphic data from the valley-confined PDC deposits  
472 collected in the Gendol channel in summer 2011, only two valley-confined PDC units reached that far  
473 downstream during the 5 November events (mBLA4 and mBLA5 units in Charbonnier et al., 2013).  
474 Based on stratigraphic correlations between the valley-confined and unconfined deposits, only the  
475 uppermost valley-confined unit (mBLA5) produced the main overspill flow unit that reached  
476 Bakalan, while the lowermost one produced the surge layers found at the base of the unconfined  
477 deposit stratigraphy.

#### 478 3.2.4 Dynamics

479 The height of the unconfined PDC as it was emplaced remained above 10 m throughout Bakalan, as  
480 evidenced by palms and trees that were singed to their full height (e.g., Figure 3a). Just to the west of  
481 the village and on the periphery of the LEDS, partially singed trees suggest current heights for the  
482 more dilute component alone of between 5 and 10 m. Much of the structural damage to buildings in  
483 the north of Bakalan was the result of isolated high pressures associated with boulders of dome rock  
484 carried within the flow (e.g., Figure 3d). The lack of structural wall failure within the main part of the  
485 slow overspill flow suggests dynamic pressures of less than 3 kPa (following the failure calculations  
486 of Jenkins et al., 2013). Maximum PDC velocities, assuming a dense PDC density of 1000 kg/m<sup>3</sup> (Druitt  
487 et al. 2002, Dufek et al. 2015), were relatively slow at 2.5 m/s (Equation 1):

$$488 \quad V = \sqrt{\frac{2q}{\rho}} \text{ (Equation 1)}$$

489 Where  $V$  = velocity (m/s),  $q$  = dynamic pressure (Pa),  $\rho$  = density (kg/m<sup>3</sup>). The overspill flow that  
490 entered Bakalan from the north appears to have been relatively low in temperature, at 100 to 200 °C.  
491 A number of thermal indicators could be used to infer emplacement temperatures of the LEDS (see  
492 Section 3.3.4) while for the dense flows, temperatures were constrained from the presence of little  
493 to no charring or blackening of timber roof supports (<200 °C: Barcík et al., 2014) and the presence  
494 of deformed polyethylene plastic pipes within the upper part of the flow deposits (>100 °C). PDC  
495 deposits to the south of Bakalan, but closer to the Gendol channel, remained at 180 °C during field  
496 studies carried out 34 days after emplacement, supporting the relatively low flow temperatures  
497 estimated within Bakalan. These temperatures are low relative to some dense unconfined deposits  
498 from other eruptions, with deposits from the June 1997 Soufrière Hills eruptions measured in the

499 days to weeks after the event at over 400 °C (Cole et al. 2002), though unconfined deposits from the  
500 2015 dome collapse events at Colima (Mexico) show temperatures from 180 to 220 °C (Pensa et al.  
501 2018). Lower temperatures at Merapi in 2010 may reflect entrainment of air over the long travel  
502 distance and interaction of PDCs with dense, tropical vegetation, while other factors could include  
503 the relatively small magma volume, the effect of topography in entraining cooler, ambient air close  
504 to source, and/or the high moisture content of the PDCs due to the summit hydrothermal system  
505 saturating the source dome rock (Jenkins et al., 2013; Komorowski et al., 2013).

### 506 **3.3 Low-energy detached surge: Bronggang**

#### 507 *3.3.1 Generation*

508 The channel constriction caused by the sabo dam and upstream concrete levees, in addition to a slight  
509 bend in the river channel towards the east at the northern edge of Bronggang village (Figure 2), are  
510 thought to have promoted surge detachment from the parent channel-confined flow (Jenkins et al.  
511 2013). LEDS then propagated around 6 to 8 m down the concrete levees and extended laterally 25 to  
512 135 m into Bronggang via three different entry points. Numerous deeply charred logs and embers  
513 were left piled up on the top of the concrete sabo walls that run alongside the Gendol channel,  
514 marking where the surges detached (Figure 4). A few small logs were carried down into the villages,  
515 potentially bending or knocking down banana trees as they collided into them down the incline. A  
516 more concentrated PDC lobe overspilled for a very short distance of about 20 m directly over the  
517 highest part of the sabo wall but at the location of maximum channel curvature, where the levees  
518 constrict at a 45° angle towards the centre of the Gendol river channel. Although the presence of this  
519 wall and constriction in the channel strongly controlled and even triggered early PDC overspill into  
520 the lower part of Bronggang, our fieldwork showed that only three out of four or potentially five  
521 surges associated with valley-confined PDCs overspilled at that location.



522  
523 *Figure 4: Photos taken from the top of the concrete levee bordering the Gendol and adjacent to*  
524 *Bronggang village: a) Looking southwest down the levee and in the direction of LEDS spillover into*  
525 *Bronggang village; b) Looking north up the infilled Gendol channel with LEDS and small flow overflow*  
526 *into Bronggang to the left of the image. Charred tree branches and embers that were carried within the*  
527 *PDC can be seen on top of and within deposits in the channel and in the village. Photos taken by S.F.*  
528 *Jenkins 25 days after impact on 30 November 2010.*

### 529 3.3.2 Impacts

530 Direct damage from the LEDS was minimal, with buildings remaining largely intact but interior and  
531 exterior plastic melted, furniture charred and paper singed. Although the LEDS were not hot enough  
532 to directly ignite these flammable objects, fire was the cause of total and partial destruction of  
533 buildings in the village. Of the 48 buildings impacted by LEDS in Bronggang, seven timber buildings  
534 were completely destroyed and a further five masonry buildings, with timber frame and tiled roofs,  
535 partially destroyed, all by fire rather than direct damage from the LEDS (Figure 5a). Firebrands  
536 (embers from burning logs within the parent PDC) carried within the surge ignited flammable  
537 materials such as hay in animal sheds and sticks and coconut husks in outside lean-to wooden  
538 kitchens (Figure 5b), with fires beginning in these flimsy wooden structures and then rapidly  
539 spreading into the adjacent houses. The large ventilation gaps also allowed firebrands to travel with  
540 the ash inside several houses, as evidenced by ignited mattresses or sofas, which smouldered without  
541 causing the houses to catch fire (Figure 5c). In one building, a small rupture in the gas tank of a  
542 motorbike stored inside greatly increased the availability of fuel leading to a fire that completely  
543 destroyed the building.

544 Prior to the eruption, ~400,000 people were rapidly evacuated to emergency shelters (Surono et al.  
545 2012) and ~1 million were otherwise displaced (Lavigne et al. 2011), but in distal villages like  
546 Bronggang many people had not evacuated at the time of the paroxysm. Out of 59 people remaining

547 in the surge zone, all of whom received burns, there were only 5 survivors. Those who were caught  
548 outside had little protection and most would have died instantly (Baxter et al., 2017); however, large  
549 ventilation pathways meant that the Leds readily entered buildings and twenty-five bodies were  
550 retrieved by rescuers from inside houses. A further 18 bodies were found outside, and 11 others died  
551 in, or on the way to, hospital (Figure 5a, Jenkins et al., 2013, Baxter et al., 2017). Some of the victims  
552 received burns from running in the deposits as they tried to escape and a cow was found alive at the  
553 time of the first rescue mission, approximately two hours after impact, but subsequently died. The  
554 last living person was rescued by approximately 06:00 (local time). Specifics of the injuries suffered  
555 by the burn victims are described in medical detail by Baxter et al. (2017). Survival of hospitalized  
556 patients was tied closely to quality of medical care, as resources in some cases were insufficient (e.g.,  
557 ventilators for treating inhalation injuries) (Baxter et al. 2017).

558

559



560

561 *Figure 5: a) Spatial distribution of building type, fire damage and casualties in a section of Bronggang*  
 562 *village (inset in Fig 2), ~13.5 km from the summit and subject to Leds. Leds flow direction across sabo*  
 563 *walls is indicated by white arrows with the white dashed line marking the sabo concrete levees*  
 564 *bordering the Gendol channel, b) remains of a burned and charred timber-framed building that was*  
 565 *totally destroyed by fires caused by Leds (Photo taken by S.F. Jenkins 28 days after impact on 3*  
 566 *December 2010), c) straw mattress burned by an isolated fire as a result of Leds inundation (Photo*  
 567 *taken by S.F. Jenkins 29 days after impact on 4 December 2010). The location of the images in (b) and*  
 568 *(c) are marked by the corresponding letters in (a).*

### 569 3.3.3 Deposits

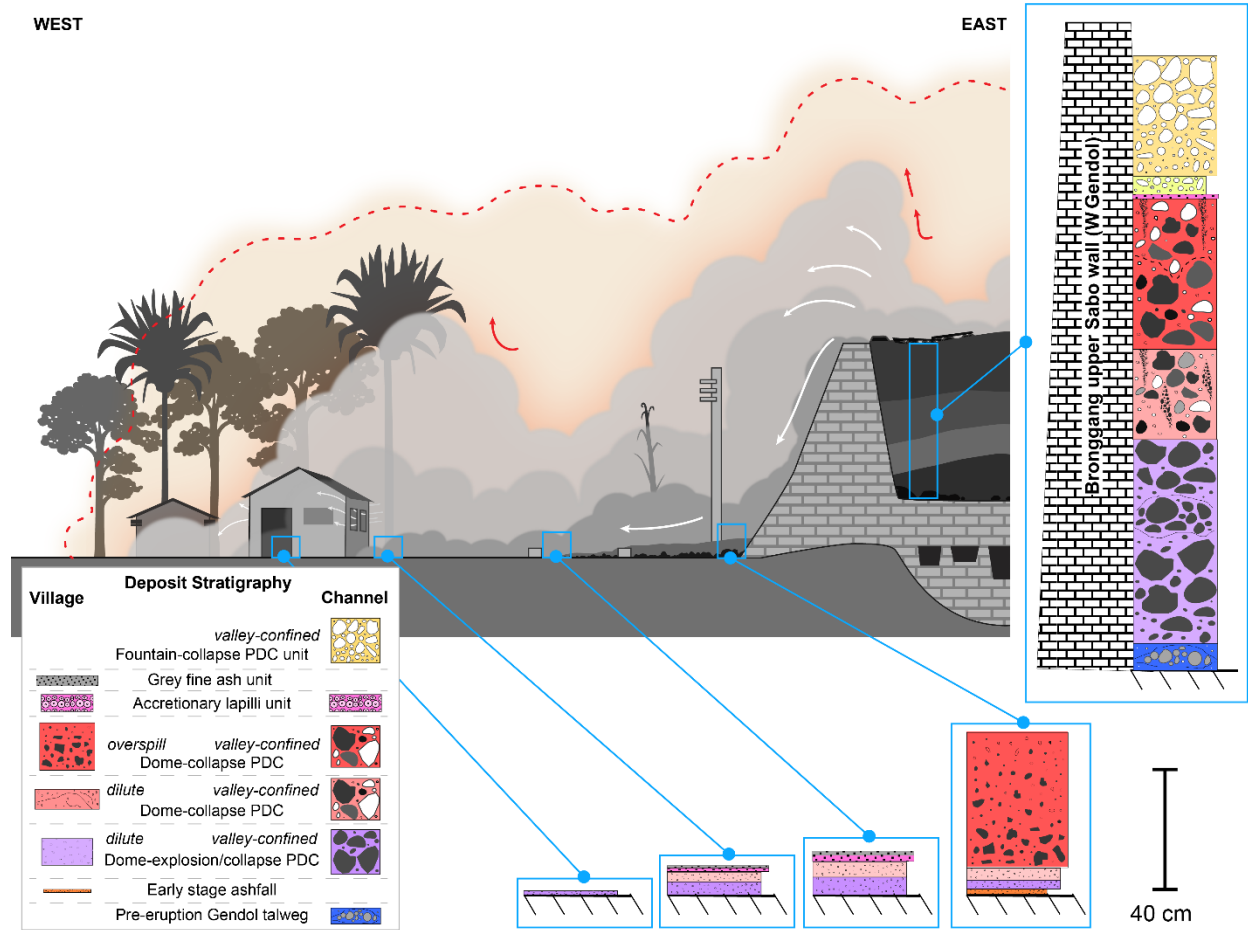
570 We identified a complex stratigraphy at the base of the sabo wall, just inside the village of Bronggang,  
 571 consisting of four different main depositional units (Figure 6):

- 572 • At the base of the sequence, there were patches of dry very fine grained, very well-sorted, loose  
 573 grey ashfall deposit 1 cm thick, which we interpreted as pre-5 November tephra erupted between  
 574 26 October and 4 November. This overlays pre-eruption soil and vegetation.

- 575 • The next unit was whitish-grey massive, coarse to fine ash, loose, poorly sorted and 3-4 cm thick  
576 with chunks of charcoal and a burnt odour. We interpreted this unit as a LEDS deposit  
577 contemporaneous or correlated to one of the surge units seen in the main Gendol channel. This  
578 unit contained pieces of aluminium foil, house tiles, and dried to scorched leaves. It was overlain  
579 by a 2 cm thick very fine-grained pinkish-tan ashfall layer.
- 580 • The third unit was a dark grey, fine ash, massive, well-sorted and normally graded 4 cm thick unit  
581 with chunks of charcoal and a locally erosive lower contact. We interpreted this unit as a second  
582 LEDS deposit contemporaneous or correlated to one of the surge units seen in the main Gendol  
583 channel. It was again overlain by a 1 cm thick, very fine grained, pinkish-tan, ashfall layer.
- 584 • The uppermost unit was a very poorly sorted, massive, compact, pinkish brown, normally to  
585 symmetrically and even reversely graded, 35-45 cm thick fines-rich unit. This unit contained  
586 large dense clasts up to 23 cm in diameter scattered on the top surface and also formed a central  
587 coarser clast-rich zone with a more pinkish matrix. We interpreted this unit as resulting from a  
588 minor overspill lobe of a valley-confined, block-rich PDC. Field evidence suggests that this PDC  
589 was not very mobile and was stopped by the ~30 cm tall stone-wall curb of the main village road  
590 on the Gendol side (Figure 6). This unit was correlative and thickened to a 93 cm thick sequence  
591 directly on top of the sabo wall. It was overlain by a 5-6 cm thick, very well-sorted, massive, fine  
592 pinkish tan ashfall layer with a vesicular texture and perhaps some poorly preserved  
593 accretionary lapilli.

594 We interpreted these deposits as representing three different minor PDC overspills, and associated  
595 ash cloud fallout, from the Gendol main channel: the lower two represent deposition from the dilute  
596 surge component only, while the upper unit includes deposition from the dense flow component as  
597 well, although this did not propagate as far as where the buildings are in the village. Parent PDCs  
598 remained largely channelized in the Gendol. LEDS depositional units were visible outside of the  
599 buildings, although only the very fine ash component of LEDS infiltrated inside (Figure 6). No  
600 stratification in deposits could be seen inside the buildings, suggesting that only one of the LEDS  
601 infiltrated, or the material was lofted and well dispersed so that it settled out gradually into one  
602 massive unit of up to 2 cm thickness that coated items inside the building (Figure 6).

603



604

605 *Fig 6: Schematic demonstrating the dynamics of Leds as it leaves the channel and inundates Bronggang*  
 606 *with stratigraphy of channel-confined, overspill and Leds deposits in and adjacent to Bronggang, ~13.5*  
 607 *km from the volcano summit.*

608 **3.3.4 Dynamics**

609 Evidence from the height of scorching on trees in the village indicated that the dilute current was at  
 610 most about 8-10 m high above the village (2 to 4 m above the levee tops). In Bronggang, at the base  
 611 of the concrete levee bordering the Gendol channel, a concrete utility pole of ~ 7.5 m high showed  
 612 pockmarks, from small clasts within the Leds striking the pole, of ~10-20 mm diameter and a few  
 613 mm deep along the full height of the pole on the upflow side (Figure 7a). The boundary between the  
 614 area of scorched, dried vegetation and pristine vegetation was very sharp, developing over less than  
 615 1 m. Figure 7b shows a traditional Javanese building at the very periphery of the Leds affected area  
 616 in Bronggang, where ash adhered to the wall of the building facing the flow, and nearby vegetation  
 617 dried and singed to a height of approximately 5 m, with some tiles dislodged on the roof overhang.  
 618 Vegetation and building components to the side and back of the building (farther from the flow) were  
 619 unaffected. Thus, at the edge of the surge, as evidenced by the vegetation patterns (Figure 7b), the

620 LEDS height was still about 5 m. Taking the maximum LEDS height of 8-10 m and maximum deposit  
621 thicknesses of ~4 cm (Section 3.3.3) gives a crude estimated maximum LEDS density of ~4 to 5 kg/m<sup>3</sup>  
622 (conservatively assuming a 1000 kg/m<sup>3</sup> deposit density as for Soufrière Hills: Druitt et al., 2002).  
623 Previous estimates of LEDS densities are rare, but for comparison, Druitt et al. (2002) estimated that  
624 in the June 1997 Soufrière Hills eruption, LEDS moving at up to 20 m/s likely had a density of 1.4  
625 kg/m<sup>3</sup> and a particle concentration below 0.1 vol%, and Bursik et al. (1998) estimated distal surges  
626 in the 1980 Mt. St. Helens eruption to have a density of 1.5 kg/m<sup>3</sup>.



627  
628 *Figure 7: a) ~7.5 m high concrete utility pole at the base of the concrete levee bordering the Gendol*  
629 *channel showing pockmarks on the upflow side, from small clasts carried within the LEDS striking the*  
630 *pole; b) Traditional Javanese building at the edge of Bronggang village showing the very sharp LEDS*  
631 *boundary, with ash and dried vegetation from the LEDS visible on just the upflow (left of image) wall*  
632 *and surrounds; c) Roof tiles lifted on the overhang of a building facing the direction of LEDS overspill*  
633 *suggesting dynamic pressures of ~0.1 to 0.2 kPa; d) Corrugated plastic roofing sheets melted by the*  
634 *LEDS and/or the deposits suggesting temperatures of at least 100 °C sustained for ~three minutes.*  
635 *Photos taken by S.F. Jenkins, November 2010.*

636 Maximum velocities of 10 m/s for the LEDS as they spilled over the concrete levee can be derived by  
637 applying the super-elevation equation (Equation 2) to the estimated 5 m high concrete levee that  
638 would need to have been overbanked by the LEDS associated with the first overflowing PDC in the

639 Gendol. This represents the maximum possible velocity of the LEDS at their point of overspill from  
640 the channel—in reality, the LEDS would likely have had lower velocities as they entered the village.  
641 Subsequent LEDS would have required lower velocities in order to overspill after previous PDCs  
642 infilled the channel, and the LEDS velocity likely rapidly attenuated with distance away from the  
643 channel. At the site of overspill, a velocity of 10 m/s correlates to a maximum dynamic pressure of  
644 ~0.2 to 0.25 kPa, assuming the previously estimated density of ~4 to 5 kg/m<sup>3</sup>. These values represent  
645 upper estimates as the pre-PDC channel infill likely banked up on the western wall of the channel, so  
646 that the overspill height is overestimated. These pressures are consistent with lack of significant tree  
647 blowdown, as even minor blowdown requires 0.5-0.8 kPa of dynamic pressure (Valentine 1998),  
648 which at our estimated densities would require a minimum velocity of ~14-16 m/s to generate.

649  $V = \sqrt{2gh}$  (Equation 2)

650 Where  $V$  = velocity (m/s),  $g$  = gravity (m/s<sup>2</sup>),  $h$  = height of barrier to overcome (m).

651 Some of the standing trees within the village showed light blackening of the bark on the side facing  
652 the surge, and their leaves were killed, but the branches remained intact reflecting the low dynamic  
653 pressures. Buildings showed limited evidence of mechanical impact: tiles on overhanging parts of  
654 roofs facing the channel were blown off by the LEDS being deflected upwards as it hit the wall (Figure  
655 7c). For only the tiles on the overhang to be lifted, the pressure upwards must exceed the weight of  
656 the tile in this location but not in other parts of the roof (BSI, 1996), which we calculate required  
657 dynamic pressure of 0.1 to 0.2 kPa. Similarly, low dynamic pressure values can be calculated for the  
658 concrete utility pole to remain upright (<0.5 kPa) and a small number of palm trees to be beheaded  
659 but not felled (< 0.5 kPa: Jenkins et al., 2013). There was likely a rapid drop off in pressures as the  
660 LEDS moved laterally farther from the channel, with no evidence of elevated pressures beyond 40 m.  
661 LEDS in Bronggang were therefore not very turbulent given the low dynamic pressures and limited  
662 lateral propagation.

663 Evidence for the thermal effects of the LEDS was complicated by the presence of fires (Figure 5), but  
664 a number of effects to objects away from the fires could be used to narrow down a likely LEDS  
665 temperature of 200 to 300 °C: i) Window glass cracked but did not melt (70 to 700 °C); ii) Healthy  
666 vegetation dried and singed, but did not ignite (100 to 400 °C); iii) Casualties suffered deep burns to  
667 uncovered skin (>150 °C: Baxter et al., 2017); iv) Acrylic roof sheets deformed (>160 °C) (Figure 7d);  
668 v) Thinner nylon clothes melted but did not auto-ignite (200 to 300 °C). This temperature range is  
669 low compared to some instances of LEDS recorded at other volcanoes (e.g., LEDS in the June 1997

670 Soufrière Hills eruption likely reached temperatures over 400 °C; Loughlin et al. 2002a), though  
671 similar to LEDS temperatures estimated in the 1994 Merapi eruption (Voight and Davis 2000).  
672 Possible reasons for the lower temperature LEDS in this eruption likely mirror the reasons for lower  
673 temperature overspill deposits, as discussed in Section 3.2.4.

674 The multi-disciplinary analysis of the Merapi 2010 eruption was the first of its kind making use of  
675 geological, engineering and medical expertise together to reconstruct PDC dynamics. The eruption  
676 also differed from prior eruptions because of the sheer number of social and professional media  
677 images of the impacts that became immediately available. These remotely sourced images, plus  
678 satellite imagery, provided a valuable source of additional information that could be evaluated to: i)  
679 infer conditions and impacts as close to the time of PDC inundation as possible, ii) assess impacts  
680 over the total PDC impacted area of ~22 km<sup>2</sup>, and iii) identify locations where field studies should  
681 focus. We were able to apply the lessons learned from the remote and field assessment of Merapi's  
682 unconfined PDCs to make a similar assessment of unconfined PDCs produced by the Fuego 2018  
683 eruption in Guatemala.

#### 684 **4 The 2018 Volcán de Fuego eruption**

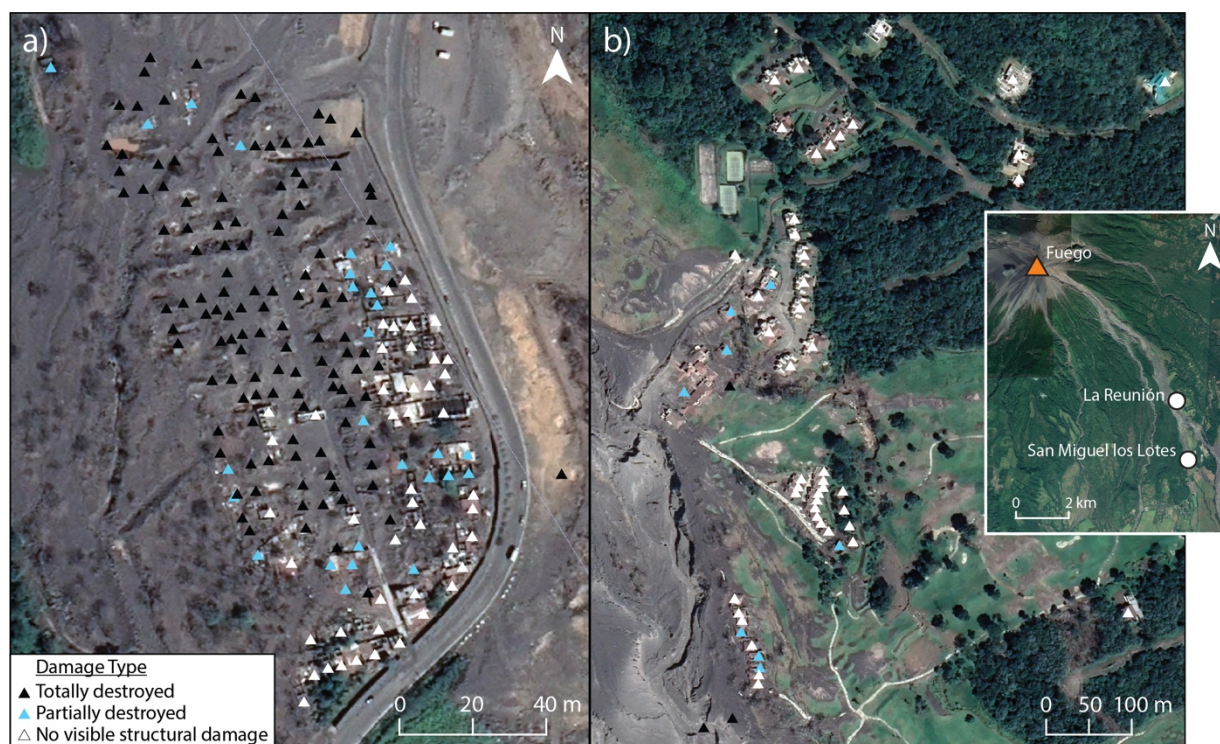
685 Unconfined PDCs during the Fuego 2018 eruption in Guatemala destroyed an estimated 750  
686 buildings in areas within 8.5 km of the volcano and resulted in at least 332 people killed or missing  
687 (with independent estimates of up to 2,900 deaths) (Naismith et al. 2020). The Fuego eruption of 3  
688 June 2018 began at 06:00 local time (UTC-6) with paroxysms from the summit vent and PDCs  
689 traveling down the western flanks, largely consistent with the volcano's previous eruptive history  
690 (Naismith et al. 2019, Pardini et al. 2019). Activity intensified by 12:00 local time, generating a series  
691 of PDCs that propagated over 11 km down Barranca Las Lajas to the southeast between 14:00 and  
692 16:00 (Naismith et al. 2019). The flow volume could not be contained by the barranca and overspilled  
693 the eastern banks of the Las Lajas channel at ~7 km from the summit at the site of La Reunión golf  
694 resort, which had been previously evacuated, as well as the western bank of the channel at ~8 km  
695 from the summit, where the channel constricted and there was a sharp bend towards the east. This  
696 latter overspill inundated the village of San Miguel los Lotes (located at ~9 km from the summit),  
697 which was still inhabited at the time (Flynn and Ramsey 2020). As the PDC struck on a Sunday, many  
698 people were congregated at church or at homes and were not working outside of the town. Further  
699 PDCs in the Barranca Las Lajas hampered rescue operations two days later on 5 June but remained  
700 contained within the channel. Fifty badly burnt casualties caught in dilute PDCs were admitted to

701 hospital, with some urgently transferred by air for treatment in specialist hospitals in the USA and  
702 Mexico.

703 A field assessment of deposits from the 2018 Fuego eruption in San Migueles los Lotes, La Reunión,  
704 and the adjacent channels was carried out in August 2018, ~3 months after the May eruption [by  
705 SJC]. The focus of the field visit was on geological deposits, but ancillary information on impacts was  
706 collected where possible, mostly in the form of photographs and field notes. A health-focused  
707 assessment was undertaken in June 2018 at the invitation of the Pan-American Health Organization (by  
708 PJB). As with Merapi, there were a large number of - sometimes graphic - images available from social  
709 and professional media in the hours, days and weeks following the June 2018 PDCs. We collected as  
710 many images as possible, broadly categorising them into deposits, impacts and casualties, and further  
711 cataloguing each image according to information it may provide regarding PDC dynamics such as  
712 velocity, dynamic pressure or temperature. We also used pre- (March 2018) and post-eruption  
713 (November 2018) Google Earth satellite imagery, and georeferenced high-resolution satellite images  
714 acquired in the days following the eruption and made available online (e.g., Digital Globe imagery  
715 acquired on June 7, 2018: White, 2018) to map pre-eruption building locations, and subsequent post-  
716 eruption damage. We followed the damage categories applied by Jenkins et al. (2013) for Merapi:  
717 Totally Destroyed (TD) where the building was not visible in post-eruption images, Partially  
718 Damaged (PD) where some of the building structure remained and could be seen in post-eruption  
719 images, and No Visible Structural Damage (NVSD) for buildings that appeared unaffected in satellite  
720 imagery. A total of 125 TD, 35 PD and 95 NVSD buildings were observed across La Reunión golf resort  
721 (3 TD, 8 PD, 47 NVSD) and San Miguel Los Lotes (122 TD, 27 PD, 48 NVSD) (Figure 8). The later Google  
722 Earth imagery, acquired ~5 months after the eruption, showed that most roofing material (metal  
723 sheets) in San Miguel los Lotes had been scavenged from PD and NVSD buildings in the intervening  
724 months (Fig 8a). From satellite and media imagery of the two overspill locations, we were able to  
725 identify at least two types of unconfined PDC, and their impact:

- 726 1. Overspill flows, of variable speed, which contained large (>2 m diameter) boulders that caused  
727 non-uniform building damage, and were responsible for almost all buildings in the TD and PD  
728 categories at both locations, with media images indicating a small number of buildings may have  
729 been inundated without causing damage;
- 730 2. Low-Energy Detached Surges (LEDS), which for the most part caused little thermal or mechanical  
731 damage, resulting in primarily buildings in the NVSD category, even though they were still fatal  
732 for at least some of the victims caught in them.

733



734

735 *Figure 8: Remotely mapped building damage for the two main flow overspill locations of a) San Miguel*  
 736 *los Lotes, and b) La Reunión golf resort, following the Fuego 2018 eruption. Google Earth satellite*  
 737 *imagery from November 2018 is shown although we assessed damage using a range of remote sourced*  
 738 *imagery. Inset shows locations relative to Fuego volcano.*

#### 739 **4.1 Impacts**

740 At La Reunión golf resort, the main club building was partially inundated with unconfined PDC  
 741 deposits and appears to have obstructed the dense component of the PDC, with only isolated lobes of  
 742 the dense flow extending downflow towards the southeast onto the golf course (Figure 9c). The main  
 743 clubhouse sustained structural damage on the upflow side (Figure 9c), and some individual  
 744 residences sustained partial damage from fires that caused roof collapse, but only three buildings  
 745 were totally destroyed, two of which were less than 50 m from the channel edge (Figure 8b). Inside  
 746 buildings, there was evidence of slow overspill flow inundation that left deposits of 80 cm or more,  
 747 with associated surges that left deposits of a few centimetres (Figure 9b). Media images (22 June  
 748 2018) showed subsequent inundation of lahars and debris that left ~50 cm-thick deposits and moved  
 749 chairs and tables: these could be distinguished from PDC deposits in media images by: i) the  
 750 increased debris (e.g., branches, bricks) that they carried, ii) evidence of deposit surface  
 751 remobilisation, iii) that they were clearly wet in comparison with photos of pristine PDC deposits,

752 and iv) the correlation with mechanical impact above the flow (lahars not imparting any mechanical  
753 impact above their flow surface: Figure 9a).

754 Approximately two-thirds of the northwestern area of the village of San Miguel Los Lotes was almost  
755 totally destroyed by overbank PDCs on 3 June (Figure 8a), which contained large boulders many  
756 metres in diameter inside an ash matrix and left massive, poorly sorted deposits up to 2 or more  
757 metres deep (Figure 9d and e). A small number of buildings at the northern end of the town escaped  
758 total destruction, and buildings at the edge of the zone of total destruction towards the south and  
759 east of the town mostly suffered partial damage, but their structures were still identifiable on satellite  
760 imagery (Figure 8a). The portion of the main road running along the south-east and east side of the  
761 town (RN-14) was completely inundated, although access to the very southernmost part of the village  
762 was maintained.

763 Most buildings at the golf course and at the far southern and eastern periphery of San Miguel Los  
764 Lotes remained relatively intact with no damage visible in satellite imagery. Media images taken  
765 during rescue operations show that people died in LEDS affected areas in San Miguel los Lotes where  
766 there was little thermal or mechanical damage to buildings. However, the majority of casualties in  
767 the village were buried inside the thick overbank PDC deposits that entered houses and buildings,  
768 creating issues to recover the bodies and correctly evaluate the human impact of the eruption.

769



Satellite image of La Reunión golf course clubhouse showing post-eruption PDC deposits (6 June, 2018; Digital Globe)

Aerial image of San Miguel los Lotes taken from the north end of town, facing south, with destroyed buildings, PDC deposits, and large boulders visible (5 June, 2018; Associated Press)

Photograph of partially buried building in San Miguel los Lotes with large boulder sitting in front of the building (7 June, 2018; Associated Press)

770  
 771 *Figure 9: a) inside of La Reunión clubhouse building showing effect of LEDES (ash-covered bottles on*  
 772 *counter) and post-eruption lahars (knocked over chairs) (22 June, 2018), b) inside of clubhouse building*  
 773 *showing overspill deposits to chair height, LEDES deposits of a few centimetres on tables, isolated fire*  
 774 *damage to roof, and ceiling fan melted due to radiant heat from overspill deposits (22 June, 2018); c)*  
 775 *Digital Globe satellite imagery of La Reunión golf resort (acquired three days after impact on 6 June,*  
 776 *2018) showing partially inundated clubhouse building. Different shade of grey between left and right*  
 777 *side of the buildings shows deposition areas of dense overspill flows (L) which were stopped by*  
 778 *structures and LEDES (R) which were able to flow past; d) aerial photo of San Miguel los Lotes, facing*  
 779 *south, showing fully destroyed northern end of town (bottom of frame) with large boulders, contrasted*  
 780 *with mostly undamaged buildings at the south end of town (top left of frame) (AP, 5 June, 2018), e)*  
 781 *partially buried building in San Miguel los Lotes with large boulder carried by dense overspill flows (AP,*  
 782 *7 June, 2018). (Reproduction rights for c-e to be purchased from the appropriate copyright holder upon*  
 783 *article acceptance.)*

784 **4.2 Inferred dynamics**

785 The maximum height of the PDCs was not easy to determine from media images. There were a  
786 number of tall (>10 m) trees in both affected areas that appear singed by the PDC, implying a current  
787 height of more than 10 m as the PDC entered the town and golf resort. Media videos of the PDC  
788 flowing past a bridge in the adjacent channel just to the south of San Miguel los Lotes suggest that  
789 current heights maintained similar heights in the channel. However, trees in the southern half of San  
790 Miguel Los Lotes and towards the peripheries of impacted areas at La Reunión golf resort were not  
791 singed to their full height, with canopies still showing as green and unaffected in satellite imagery  
792 while the full height of buildings was affected. Thus, the total PDC height decreased from >10 m to  
793 between 2 to 10 m as the flow slowed down and came to a stop.

794 At the golf resort, the energy of the overspill flows was low enough that they could be largely blocked  
795 by buildings, and where the flows entered buildings, they only moved objects such as chairs a few  
796 tens of centimetres away with the associated surges leaving countertop items such as bottles coated  
797 in ash but upright (Figure 9a). This suggests that both the dense and dilute PDC components were  
798 traveling at ~1 m/s (certainly less than 5 m/s based on the categories outlined in Figure 1) with  
799 minimal dynamic pressures (< 0.2 kPa). LEDES at the golf resort maintained similarly low velocities  
800 and dynamic pressures, evidenced by their ability to fell only slim and very small (2-3 m height) trees  
801 or palms, but not to remove roof tiles or to move items located on tables inside buildings. Some media  
802 images showed wall and roof damage at the golf resort, and field investigation confirmed structural  
803 damage to the main clubhouse from PDCs, while most of this damage to other buildings seemed to be  
804 the result of post-eruption lahars (wall damage) and fire events (roof damage), rather than direct  
805 damage from PDCs (Figure 9b).

806 In San Miguel los Lotes, the overspill flows likely decreased in velocity and dynamic pressure as they  
807 moved south and east in order for the buildings in these parts of town to sustain minimal to no  
808 observable damage. The widespread destruction of most buildings at the northern part of the town  
809 along with a few surviving buildings of the same typology (Figure 8a) suggests that destruction of  
810 buildings was caused by a combination of dynamic pressure and missile damage from large clasts  
811 carried by the flows. Many large boulders of 2 m diameter or more can be seen in and near the north  
812 end of town in post-eruption photos (Figure 9d and e) and satellite imagery. LEDES in San Miguel Los  
813 Lotes appeared to have low velocity and dynamic pressure (<0.5 kPa), evidenced by the fact that  
814 many trees (including palms) within the village remained standing and metal roof sheets remained  
815 attached to the roof framing after the event.

816 Isolated fire damage could be seen in some of the buildings at the golf course and in San Miguel Los  
817 Lotes, leading to partial or total roof collapse in places. It is not clear from remotely derived imagery  
818 if isolated fires were the result of embers carried within the PDC, as at Merapi, or related to the heat  
819 of the deposits. Flow deposits at Fuego contained large boulders, but field studies showed that most  
820 of these boulders were not juvenile, and therefore unlikely to have provided a concentrated heat  
821 source that may also have triggered fire.

822 Photos from the rescue operation in San Miguel los Lotes show that the PDC deposits were hot  
823 enough that it was necessary for responders to lay boards down to walk on in some locations, and  
824 there were reports of responder's shoe soles melting (World Bank 2018). These suggest deposits of  
825 at least 100°C, but likely much higher. In one media photo from the interior of a golf course building,  
826 chair bases and plastic ceiling fans were melted, and we infer this is the result of radiant heat from  
827 the flow deposit rather than the heat associated with the surge (Figure 9b). For LEDS, media photos  
828 from both the golf course and the town indicate relatively low temperatures for the most part  
829 (maximum 100-200 °C). Fragile items such as plastic plant pots and bags are not deformed or melted,  
830 and in available media images there is no evidence for cracked glasses and only very slight melting  
831 to thin nylon clothing (>70 °C). Additionally, media images showed plants that remained alive, and  
832 were not dried out, singed or charred by the passing LEDS. This suggests temperatures of around 100  
833 °C or less, significantly lower than in more proximal areas (<5 km), where photos from the field  
834 studies show significant singeing and burning of trees and coffee plants. However, by contrast, some  
835 media images showed casualties in a pugilistic attitude with clothing intact, indicating fourth degree  
836 burns that have penetrated below the skin layer to involve the limb muscles (at least 200 °C) (Baxter,  
837 1990). Not all casualties displayed this attitude, despite wearing similar clothing (t-shirt and  
838 trousers) and being affected by LEDS in the same town. Since there was no observed evidence of fires  
839 near these casualties, the temperatures necessary to cause these injuries can be attributed to the  
840 LEDS. The evidence from thermal effects therefore suggests that there was variability in temperature  
841 and/or duration of the impact across the impacted area, reflecting the uneven inundation of PDCs  
842 across the village area.

843 While remotely assessing impacts visible in satellite, aerial and media images in this case study was  
844 valuable, access to photos and on-the-ground experience in the aftermath of the Fuego eruption  
845 provided vital detail that allowed us to confirm or refute inferences made from media images and  
846 added information not visible in remote imagery. Ideally, remote and field approaches are combined,  
847 with remote approaches providing information on the immediate post-impact situation and for areas

848 that cannot be easily accessed as well as providing the larger scale overview, which can then be  
849 refined and ground-truthed with informed field visits that provide more detailed information,  
850 background and context. Studies relating impacts and PDC dynamics with the deposits provide an  
851 evidence base from which likely PDC dynamics and impacts can be forecast. This is particularly  
852 important for volcanoes where there are no data on past eruptions, or where the only data available  
853 are past deposits.

## 854 **5 Discussion and conclusions**

855 In this study, we reviewed the physical characteristics and devastating impact associated with  
856 unconfined PDCs. We identified four unconfined PDC end-member types: i) Fast overflow flow; ii)  
857 Slow overflow flow; iii) High energy surge; and iv) Low energy detached surge, all four of which were  
858 produced by the 2010 Merapi eruption, Indonesia. We used previously unpublished data on the  
859 deposits and impacts of slow overflow flows in Bakalan village, 12.6 km from the summit, and LEDS  
860 in Bronggang village, 13.5 km from the summit, to infer some key characteristics of their  
861 emplacement dynamics. Using the lessons learned from Merapi, we then applied the same approach  
862 using remotely sourced imagery (satellite images, social and professional media) and field studies to  
863 assess impacts and infer the dynamics of unconfined PDCs produced during the Fuego 2018 eruption.  
864 The deposits, impacts and dynamics associated with the unconfined slow overflow flows and low  
865 energy detached surges produced during the case study eruptions of Merapi and Fuego fall within  
866 the range of those observed or inferred in previously recorded events (Table 1 and Section 2). Broad  
867 conclusions can thus be drawn about the key characteristics and impacts of unconfined PDCs:

- 868 1. Destruction of buildings, vegetation and infrastructure is typically complete in the main path of  
869 fast overflow flows and high-energy surges;
- 870 2. A rapid attenuation in velocity at the peripheries of flow overflows and high-energy surges leads  
871 to reduced dynamic pressures and thus reduced mechanical impact and severity of damage. At  
872 the very peripheries of flows (slow overflow flow margin), deposits bank up against the sides of  
873 buildings or inundate the interior through open doors without causing any structural damage;
- 874 3. Low-energy detached surges are unique amongst the four unconfined PDC types in that they  
875 cause relatively little damage through dynamic pressures and leave little geological evidence;  
876 however, they are still mostly fatal because of the heat flux and should therefore be afforded the  
877 same consideration for hazard management planning as the unconfined dense flows and high-  
878 energy surges for which we may have more geological evidence;

- 879 4. The temperature of unconfined PDCs can vary greatly between eruptions, as a function of the PDC  
 880 volume, generation mechanism and transport path, as well as the presence of heat sinks such as  
 881 wet vegetation;
- 882 5. General patterns of reduced or little damage in areas where dynamic pressures were relatively  
 883 low were disrupted by isolated instances of total building damage as a result of fires or  
 884 boulders/debris transported within the flow.

885 *Table 1: The range of unconfined PDC characteristics and dynamics for each unconfined PDC type from*  
 886 *previous eruptions following the studies reported in Section 1 and 2 and this study. Values obtained for*  
 887 *the four detailed study areas of the Merapi 2010 and Fuego 2018 eruptions are shown in brackets.*  
 888 *Distances are straight-line and represent the shortest distance from impact site to summit or channel,*  
 889 *and not necessarily the distance travelled.*

Deposit thickness (at impact sites)	Dynamics				Distance to impact site	
	Height	Velocity	Dynamic pressure	Temperature	From summit	From channel
<b>Fast overspill flow</b>						
10s of centimetres <sup>a</sup> to metres <sup>c</sup>	-	30 m/s to 60 m/s	Up to 100 kPa proximal, 15 kPa distal <sup>d</sup>	Up to >600 °C <sup>a</sup>	5 km <sup>a, c</sup>	600 m <sup>e</sup> to 800 m <sup>a</sup>
<b>Slow overspill flow margin</b>						
Up to 0.5 m <sup>e</sup> [Up to ~2 m <sup>a</sup> , up to ~3 m <sup>b</sup> ]	2 m <sup>b</sup> to 10 m <sup>a, b</sup> [10 m <sup>a</sup> , 2-10 m <sup>b</sup> ]	1 m/s <sup>e</sup> to 2.5 m/s <sup>a</sup> [~2.5 m/s <sup>a</sup> , ~1 m/s <sup>b</sup> ]	<0.5 kPa <sup>b</sup> to 3 kPa <sup>a, e</sup> [<3 kPa <sup>a</sup> , <0.5 kPa <sup>b</sup> ]	100 °C <sup>a</sup> to 410 °C <sup>e</sup> [100-200 °C <sup>a</sup> , >100 °C <sup>b</sup> ]	2 km <sup>e</sup> to 12.6 km <sup>a</sup> [12.6 km <sup>a</sup> , 7 km <sup>b</sup> ]	200 m <sup>b</sup> to 300 m <sup>a</sup> [300 m <sup>a</sup> , 200 m <sup>b</sup> ]
<b>High-energy surge</b>						
<20 cm <sup>h</sup> to Meters <sup>e</sup>	-	50 m/s <sup>i</sup> to 150 m/s <sup>g</sup>	<1 kPa <sup>f</sup> to >10 kPa <sup>f</sup>	120 °C <sup>g</sup> to 350 °C <sup>h</sup>	4 km <sup>h</sup> to 30 km <sup>g</sup>	Up to 0.8 km <sup>h</sup> or n/a (blast)
<b>Low-energy detached surge (LEDS)</b>						
Few cm <sup>e</sup> to 20 cm <sup>i</sup> [<4 cm <sup>a</sup> , few cm <sup>b</sup> ]	2 m <sup>b</sup> to 10 m <sup>a, b</sup> [8-10 m <sup>a</sup> , 2-10 m <sup>b</sup> ]	1 m/s <sup>b</sup> to 10m/s <sup>a</sup> [<10 m/s <sup>a</sup> , ~1 m/s <sup>b</sup> ]	<0.2 kPa <sup>a</sup> to 2 kPa <sup>e</sup> [<0.2 kPa <sup>a</sup> , <0.5 kPa <sup>b</sup> ]	100 °C <sup>b</sup> to ~400 °C <sup>e</sup> [200-300 °C <sup>a</sup> , 100-200 °C <sup>b</sup> ]	2.5 km <sup>e</sup> to 13.5 km <sup>a</sup> [13.5 km <sup>a</sup> , 8.5 km <sup>b</sup> ]	40 m <sup>i</sup> to 450 m <sup>b</sup> [200 m <sup>a</sup> , 450 m <sup>b</sup> ]
<sup>a</sup> Merapi 2010, <sup>b</sup> Fuego 2018, <sup>c</sup> Merapi 2006, <sup>d</sup> Colima 2015, <sup>e</sup> Soufrière Hills 1997, <sup>f</sup> Mount Pelée 1902, <sup>g</sup> Mt. St. Helens 1980, <sup>h</sup> Unzen 1991, <sup>i</sup> Merapi 1994 -: Missing values could not be reasonably inferred from available literature or imagery.						

890

891 Unconfined PDCs exist on a spectrum of both concentration and velocity, which both contribute to  
 892 dynamic pressure, a key trait in determining the damage caused by a PDC. However, the temperature

893 and duration of impact is also an important component in determining impact for the less energetic  
894 PDCs. These two factors affect the chance of survival and the probability of fire ignition. It is nearly  
895 impossible to disentangle the contribution of temperature and duration in determining thermal  
896 impact. Evidence from casualties in Bronggang affected by the LEDS of Merapi 2010, suggests an  
897 LEDS duration in the region of minutes (Baxter et al., 2017, Jenkins et al., 2013). Refining estimates  
898 of duration is difficult, especially if inferred from field and remote studies alone, although  
899 sophisticated numerical models that aim to recreate the physical processes underlying PDC  
900 generation and transport can offer some insight (e.g., Esposti Ongaro et al. 2020), as may controlled  
901 experiments (e.g., Mastrolorenzo et al. 2010).

902 The range of observed characteristics across different eruptions but within unconfined PDCs of the  
903 same type (Table 1) can be related to a few potential factors. The size of the magma batch and the  
904 volume of erupted material may affect PDC temperatures at their generation, leading ultimately to  
905 differences in source temperatures between eruptions, before PDCs become unconfined. The PDC  
906 generation mechanism appears to affect the temperature of ensuing PDCs: collapsing lava domes  
907 (e.g., Soufrière Hills 1997, Merapi 1994, 2006, 2010) are correlated with higher initial PDC  
908 temperatures than a sector collapse (e.g., Fuego 2018), and this appears to play a stronger role than  
909 distance from the volcano. For example, PDCs at the affected sites near Fuego appear to have been  
910 either similar or lower temperature despite being closer to the volcano (~8 km) than the sites at  
911 Merapi (~13 km).

912 The velocity (and therefore the dynamic pressure) of PDCs seems to be strongly influenced by the  
913 cause of unconfinement. Based on recorded examples, PDCs unconfined from inception (e.g., directed  
914 blast at Mt. Pelée 1902) and those that simply outrun their valley-confined, parent flows (e.g., high-  
915 energy surges at Unzen 1991) seem capable of maintaining their high velocities (>60 m/s), while  
916 those caused by channel bends or constrictions (e.g., slow overflows and LEDS at Merapi 1994 and  
917 2010) often decrease in velocity drastically soon after leaving the channel to the speeds inferred in  
918 this study (<10 m/s). Unconfined PDCs, despite their lower velocities, can maintain high mobility,  
919 flowing kilometres downstream after unconfinement (e.g., Merapi 2010, Fuego 2018) or even  
920 reforming confined flows when encountering a new channel (e.g., Soufrière Hills June 1997). As a  
921 general rule, LEDS are the slowest-moving (a few m/s) and most dilute (<5 kg/m<sup>3</sup>) of the unconfined  
922 PDCs, resulting in the lowest dynamic pressures (<0.5 kPa) and thus the least mechanical damage to  
923 buildings. LEDS deposits are typically no thicker than 20 cm, with satellite imagery and field visits  
924 following the Fuego and Merapi eruptions showing that most of their deposits were on the order of

925 a few centimetres and had already been washed away within as little as a few weeks. The ease with  
926 which LEDS deposits can be eroded and washed away means that they are poorly preserved in the  
927 geological record. However, in all previous cases where LEDS have inundated still inhabited areas,  
928 they were hot enough to be deadly to their farthest extent.

929 LEDS are unique amongst the unconfined PDCs discussed here as they impart little mechanical  
930 impact and leave only very thin deposits but can still be fatal. A wide range of LEDS emplacement  
931 temperatures exists, with thermal impacts on plastics, vegetation and clothes suggesting relatively  
932 low temperatures of around 100-220 °C in San Miguel los Lotes, Fuego, ~200-300 °C in Bronggang,  
933 Merapi, and >400 °C in Streatham, Soufrière Hills. In Bronggang, less than 10% of the 59 people  
934 affected by the LEDS survived. It is impossible to determine the amount or percentage of casualties  
935 in San Miguel los Lotes resulting from LEDS even with an on-the-ground assessment due to the high  
936 amount of burial by the dense flows (resulting in extremely variable reporting on the death toll).  
937 Media images show that some of the deaths, especially in the southern end of town less affected by  
938 dense flows, were the result of people being caught in LEDS. In both the Merapi 2010 and Fuego 2018  
939 eruptions, LEDS deaths occurred due to severe burns and inhalation both inside and outside  
940 buildings, evidenced by bodies found in a pugilistic attitude, with clothing often intact. Flow  
941 overspills were responsible for many more deaths in the Fuego eruption than at Merapi; a complex  
942 combination of political, cultural, economic, and demographic factors, unrelated to PDC dynamics or  
943 geology, likely played an important role. San Miguel los Lotes was significantly more populated than  
944 Bakalan and was not evacuated prior to the eruption, meaning that fatality in the northern part of the  
945 village highly affected by flows would have been near total. In Bakalan, there were only four or five  
946 casualties thanks to prior evacuation. Similarly, at La Reunión, loss of life was prevented by a full  
947 evacuation prior to the arrival of PDCs.

948 Fires following the inundation of PDC can cause more damage than the PDC itself, although with  
949 dense PDCs the evidence of damage can be buried. Widespread fire following the directed blast of  
950 Pelée 1902 incinerated the town of St. Pierre, leaving no evidence of the thermal impact of the PDC  
951 itself. In all recorded LEDS, localised fires were ignited and at Merapi, this could be attributed to  
952 embers (firebrands) carried within the LEDS (Jenkins et al., 2013). It is reasonable to infer that in  
953 situations with fewer firebrands present (e.g., fewer trees consumed in the surge path), the likelihood  
954 of building damage from LEDS may be lower. Building typology is also a factor affecting the level of  
955 damage sustained during LEDS, with timber buildings much more likely to be damaged in a LEDS-  
956 caused fire than masonry buildings. Considering these factors, fire damage resulting from LEDS is

957 likely to be higher in dry areas and/or during dry seasons and in areas containing buildings made  
958 from more flammable material. Conversely, it is possible that the potential for building damage from  
959 LEDS could be diminished or discounted in arid unvegetated areas, where building types are less  
960 flammable, if flammable items are removed prior to inundation, and/or during the rainy season or in  
961 wet areas. However, the rapid inundation of multiple PDCs in a short amount of time (as at  
962 Bronggang) can act to dry out wet vegetation or other sources of fuel priming it for ignition.

963 By their nature, unconfined PDCs are difficult to forecast because they inundate areas beyond the  
964 topographic lows that are typically given priority in volcanic hazard planning. As numerical models  
965 become more sophisticated (e.g., Esposti Ongaro et al. 2008, Kelfoun et al. 2017, Lube et al. 2020),  
966 they may be better able to recreate, and therefore forecast, the path and dynamics of unconfined  
967 PDCs. In the meantime, one approach in mitigation planning has been to apply a 'buffer' (e.g., Neri et  
968 al., 2015) around a PDC-prone channel to highlight threatened populations and infrastructure, with  
969 the aim of implementing long-term land-use or short-term proactive evacuation measures for  
970 communities close to topographic lows. The extent of this buffer is difficult to define, and is a function  
971 of the channel topography, PDC volume and local PDC mass flux/velocity as well as preceding events  
972 in the eruption sequence (e.g., the infilling by previous PDC deposits). For directed blasts, a buffer is  
973 clearly not appropriate because of their wide-reaching and topography-mantling nature, in these  
974 cases an energy cone model that defines distance from the summit may be useful. For those high-  
975 energy surges that are not unconfined from origin, e.g., Unzen 1991, this type of model is less useful  
976 as it is unable to identify locations of surge detachment. For overspill PDCs, we found they reach a  
977 maximum lateral distance of 800 m (Table 1) from the flowpath channel. However, we recognise that  
978 buffer extents are likely to be unique to the specific eruptions and require consideration of the  
979 topography, channel path and likely eruptive style. Reliance on geological deposits for defining  
980 buffers and potentially hazardous areas must be cognisant of the thinner deposits that reflect  
981 unconfined PDCs that cannot be preserved but are still deadly.

982 Volcanic hazard and risk assessment relies upon empirical data from past eruptions and their  
983 impacts. However, we are often limited in the amount of data that can be collected shortly after an  
984 event, while deposits and impacts are preserved, because of safety and access limitations. In this  
985 study, we have used lessons learned from remote and ground surveys of PDC dynamics following the  
986 Merapi 2010 eruption to provide a similar assessment for Fuego 2018. Remote assessment at Fuego  
987 using satellite imagery and media images to supplement a field study allowed for many similar  
988 determinations of PDC dynamics and resultant impacts as at Merapi. In both cases, through imagery

989 or direct observation, building damage, extent of casualties, condition of vegetation, and state of  
990 materials like plastics and fabrics could be extrapolated into velocities, concentrations, dynamic  
991 pressures, temperatures, and the height of the associated PDCs. Personal familiarity with the affected  
992 area as well as presence on site allowed for more precise damage evaluation of buildings, as well as  
993 a more thorough record of geo-referenced photos than could be obtained through media images.  
994 Another vital piece of information provided by field studies is geological information. Detailed  
995 stratigraphic study and deposit analysis at Merapi was obtained over multiple field visits and these  
996 data, when combined with the impact assessment, were valuable for making inferences about PDC  
997 processes, whereas discussion of PDC dynamics at Fuego relied upon remote imagery and  
998 information from one field study, for which the focus was on deposits and not impacts. As shown at  
999 Merapi and Fuego, depending on the circumstances of the study, both remote and on-the-ground  
1000 analysis serve a vital role in inferring the PDC characteristics that inform hazard models, mitigation,  
1001 and risk assessment.

## 1002 **6 CRediT authorship contribution statement**

1003 SFJ devised the study. SFJ, SJC, PJB, and JCK performed fieldwork and/or in-person damage  
1004 assessment. GAL and SFJ curated and compiled data. GAL and SFJ performed remote hazard  
1005 assessment. GAL and SFJ wrote the first draft. GAL, SFJ, SJC, PJB, and JCK reviewed and edited the  
1006 manuscript.

## 1007 **7 Acknowledgements**

1008 GAL and SFJ acknowledge funding from AXA and Singapore National Research Foundation  
1009 (NRF2018NRF-NSFC003ES-010). This research was supported by the Earth Observatory of  
1010 Singapore via its funding from the National Research Foundation Singapore and the Singapore  
1011 Ministry of Education under the Research Centres of Excellence initiative. This work comprises EOS  
1012 contribution number 371. SFJ, PJB and JCK are grateful for funding from the European Union  
1013 (MIAVITA) and Agence Nationale de la Recherche (CASAVA). PJB acknowledges funding from the Pan  
1014 American Health Organisation. SJC would like to acknowledge NSF RAPID grant #1841852 and  
1015 colleagues from the Fuego 2018 eruption crisis response team. The authors would like to  
1016 acknowledge CVGHM, BPPTK, and INSIVUMEH for their cooperation and responses to the Merapi  
1017 2010 and Fuego 2018 eruptions. We are grateful to Nguyen Thi Nam Phuong for creating of the  
1018 schematic portion of Figure 6. We would like to acknowledge an anonymous photographer for

1019 providing the non-credited photos used in Figure 9. We are grateful to Chai Min Wei who, in the  
1020 weeks following the June 2018 Fuego eruption, collated many of the available media images.

## 1021 **8 References**

1022 Abdurachman, E.K., Bourdier, J.-L., Voight, B., 2000. Nuées ardentes of 22 November 1994 at Merapi  
1023 volcano, Java, Indonesia. *Journal of Volcanology and Geothermal Research* 100, 345–361.  
1024 [https://doi.org/10.1016/S0377-0273\(00\)00144-X](https://doi.org/10.1016/S0377-0273(00)00144-X)

1025 Anderson, T., Flett, J.S., 1902. Preliminary report on the recent eruption of the Soufrière in St. Vincent,  
1026 and of a visit to Mont Pelée, in Martinique. *Proceedings of the Royal Society of London* 70, 423–  
1027 445. <https://doi.org/10.1098/rspl.1902.0042>

1028 Barčík, Š., Gašparík, M., Razumov, E.Y., 2014. EFFECT OF TEMPERATURE ON THE COLOR CHANGES  
1029 OF WOOD DURING THERMAL MODIFICATION. *Cell Chem Technol* 49, 789–798.

1030 Baxter, P.J., 1990. Medical effects of volcanic eruptions: I. Main causes of death and injury. *Bull*  
1031 *Volcanol* 52, 532–544. <https://doi.org/10.1007/BF00301534>

1032 Baxter, P.J., Boyle, R., Cole, P., Neri, A., Spence, R., Zuccaro, G., 2005. The impacts of pyroclastic surges  
1033 on buildings at the eruption of the Soufrière Hills volcano, Montserrat. *Bull Volcanol* 67, 292–  
1034 313. <https://doi.org/10.1007/s00445-004-0365-7>

1035 Baxter, P.J., Horwell, C.J., 2015. Impacts of Eruptions on Human Health, in: *The Encyclopedia of*  
1036 *Volcanoes*. Elsevier, pp. 1035–1047. <https://doi.org/10.1016/B978-0-12-385938-9.00060-2>

1037 Baxter, P.J., Jenkins, S., Seswandhana, R., Komorowski, J.-C., Dunn, K., Purser, D., Voight, B., Shelley, I.,  
1038 2017. Human survival in volcanic eruptions: Thermal injuries in pyroclastic surges, their  
1039 causes, prognosis and emergency management. *Burns* 43, 1051–1069.  
1040 <https://doi.org/10.1016/j.burns.2017.01.025>

1041 Belousov, A., Belousova, M., Hoblitt, R., Patia, H., 2020. The 1951 eruption of Mount Lamington, Papua  
1042 New Guinea: Devastating directed blast triggered by small-scale edifice failure. *Journal of*  
1043 *Volcanology and Geothermal Research* 401, 106947.  
1044 <https://doi.org/10.1016/j.jvolgeores.2020.106947>

- 1045 Belousov, A., Voight, B., Belousova, M., 2007. Directed blasts and blast-generated pyroclastic density  
1046 currents: a comparison of the Bezymianny 1956, Mount St Helens 1980, and Soufrière Hills,  
1047 Montserrat 1997 eruptions and deposits. Bull Volcanol 69, 701.  
1048 <https://doi.org/10.1007/s00445-006-0109-y>
- 1049 Benage, M.C., Dufek, J., Mothes, P.A., 2016. Quantifying entrainment in pyroclastic density currents  
1050 from the Tungurahua eruption, Ecuador: Integrating field proxies with numerical simulations.  
1051 Geophysical Research Letters 43, 6932–6941. <https://doi.org/10.1002/2016GL069527>
- 1052 Bourdier, J.L., Boudon, G., Gourgaud, A., 1989. Stratigraphy of the 1902 and 1929 nuée-ardente  
1053 deposits, Mt. Pelée, Martinique. Journal of Volcanology and Geothermal Research 38, 77–96.  
1054 [https://doi.org/10.1016/0377-0273\(89\)90031-0](https://doi.org/10.1016/0377-0273(89)90031-0)
- 1055 Breard, E.C.P., Lube, G., 2017. Inside pyroclastic density currents – uncovering the enigmatic flow  
1056 structure and transport behaviour in large-scale experiments. Earth and Planetary Science  
1057 Letters 458, 22–36. <https://doi.org/10.1016/j.epsl.2016.10.016>
- 1058 Brosch, E., Lube, G., 2020. Spatiotemporal sediment transport and deposition processes in  
1059 experimental dilute pyroclastic density currents. Journal of Volcanology and Geothermal  
1060 Research 401, 106946. <https://doi.org/10.1016/j.jvolgeores.2020.106946>
- 1061 Brown, R.J., Andrews, G.D.M., 2015. Chapter 36 - Deposits of Pyroclastic Density Currents, in:  
1062 Sigurdsson, H. (Ed.), The Encyclopedia of Volcanoes (Second Edition). Academic Press,  
1063 Amsterdam, pp. 631–648. <https://doi.org/10.1016/B978-0-12-385938-9.00036-5>
- 1064 Brown, S.K., Jenkins, S.F., Sparks, R.S.J., Odbert, H., Auker, M.R., 2017. Volcanic fatalities database:  
1065 analysis of volcanic threat with distance and victim classification. Journal of Applied  
1066 Volcanology 6, 15. <https://doi.org/10.1186/s13617-017-0067-4>
- 1067 BSI, B., 1996. 6399-1, Loading for buildings, in: Code of Practice for Dead and Imposed Loads. BSI,  
1068 London, UK.
- 1069 Bursik, M.I., Kurbatov, A.V., Sheridan, M.F., Woods, A.W., 1998. Transport and deposition in the May  
1070 18, 1980, Mount St. Helens blast flow. Geology 26, 155–158. [https://doi.org/10.1130/0091-7613\(1998\)026<0155:TADITM>2.3.CO;2](https://doi.org/10.1130/0091-7613(1998)026<0155:TADITM>2.3.CO;2)  
1071

- 1072 Charbonnier, S.J., Germa, A., Connor, C.B., Gertisser, R., Preece, K., Komorowski, J.-C., Lavigne, F., Dixon,  
1073 T., Connor, L., 2013. Evaluation of the impact of the 2010 pyroclastic density currents at Merapi  
1074 volcano from high-resolution satellite imagery, field investigations and numerical simulations.  
1075 Journal of Volcanology and Geothermal Research 261, 295–315.  
1076 <https://doi.org/10.1016/j.jvolgeores.2012.12.021>
- 1077 Charbonnier, S.J., Gertisser, R., 2008. Field observations and surface characteristics of pristine block-  
1078 and-ash flow deposits from the 2006 eruption of Merapi Volcano, Java, Indonesia. Journal of  
1079 Volcanology and Geothermal Research, Volcanic Flows and Falls 177, 971–982.  
1080 <https://doi.org/10.1016/j.jvolgeores.2008.07.008>
- 1081 Clarke, A.B., Voight, B., 2000. Pyroclastic current dynamic pressure from aerodynamics of tree or pole  
1082 blow-down. Journal of Volcanology and Geothermal Research 100, 395–412.  
1083 [https://doi.org/10.1016/S0377-0273\(00\)00148-7](https://doi.org/10.1016/S0377-0273(00)00148-7)
- 1084 Cole, P.D., Calder, E.S., Sparks, R.S.J., Clarke, A.B., Druitt, T.H., Young, S.R., Herd, R.A., Harford, C.L.,  
1085 Norton, G.E., 2002. Deposits from dome-collapse and fountain-collapse pyroclastic flows at  
1086 Soufrière Hills Volcano, Montserrat. Geological Society, London, Memoirs 21, 231–262.  
1087 <https://doi.org/10.1144/GSL.MEM.2002.021.01.11>
- 1088 Cole, P.D., Neri, A., Baxter, P.J., 2015. Chapter 54 - Hazards from Pyroclastic Density Currents, in:  
1089 Sigurdsson, H. (Ed.), The Encyclopedia of Volcanoes (Second Edition). Academic Press,  
1090 Amsterdam, pp. 943–956. <https://doi.org/10.1016/B978-0-12-385938-9.00054-7>
- 1091 Cooper, M.J.M., 2018. The Mt. Unzen Disaster: A Terrible Learning Experience, in: Chakraborty, A.,  
1092 Mokudai, K., Cooper, M., Watanabe, M., Chakraborty, S. (Eds.), Natural Heritage of Japan,  
1093 Geoheritage, Geoparks and Geotourism. Springer International Publishing, Cham, pp. 131–142.  
1094 [https://doi.org/10.1007/978-3-319-61896-8\\_12](https://doi.org/10.1007/978-3-319-61896-8_12)
- 1095 Cronin, S.J., Lube, G., Dayudi, D.S., Sumarti, S., Subrandiyo, S., Surono, 2013. Insights into the October–  
1096 November 2010 Gunung Merapi eruption (Central Java, Indonesia) from the stratigraphy,  
1097 volume and characteristics of its pyroclastic deposits. Journal of Volcanology and Geothermal  
1098 Research, Merapi eruption 261, 244–259. <https://doi.org/10.1016/j.jvolgeores.2013.01.005>
- 1099 Dellino, P., Büttner, R., Dioguardi, F., Doronzo, D.M., La Volpe, L., Mele, D., Sonder, I., Sulpizio, R.,  
1100 Zimanowski, B., 2010. Experimental evidence links volcanic particle characteristics to

- 1101 pyroclastic flow hazard. *Earth and Planetary Science Letters* 295, 314–320.  
1102 <https://doi.org/10.1016/j.epsl.2010.04.022>
- 1103 Druitt, T.H., Calder, E.S., Cole, P.D., Hoblitt, R.P., Loughlin, S.C., Norton, G.E., Ritchie, L.J., Sparks, R.S.J.,  
1104 Voight, B., 2002. Small-volume, highly mobile pyroclastic flows formed by rapid sedimentation  
1105 from pyroclastic surges at Soufrière Hills Volcano, Montserrat: an important volcanic hazard.  
1106 *Geological Society, London, Memoirs* 21, 263–279.  
1107 <https://doi.org/10.1144/GSL.MEM.2002.021.01.12>
- 1108 Esposti Ongaro, T., Clarke, A.B., Neri, A., Voight, B., Widiwijayanti, C., 2008. Fluid dynamics of the 1997  
1109 Boxing Day volcanic blast on Montserrat, West Indies. *Journal of Geophysical Research: Solid*  
1110 *Earth* 113. <https://doi.org/10.1029/2006JB004898>
- 1111 Esposti Ongaro, T., Clarke, A.B., Voight, B., Neri, A., Widiwijayanti, C., 2012. Multiphase flow dynamics  
1112 of pyroclastic density currents during the May 18, 1980 lateral blast of Mount St. Helens.  
1113 *Journal of Geophysical Research: Solid Earth* 117. <https://doi.org/10.1029/2011JB009081>
- 1114 Esposti Ongaro, T., Komorowski, J.-C., Legendre, Y., Neri, A., 2020. Modelling pyroclastic density  
1115 currents from a subplinian eruption at La Soufrière de Guadeloupe (West Indies, France). *Bull*  
1116 *Volcanol* 82, 76. <https://doi.org/10.1007/s00445-020-01411-6>
- 1117 Fisher, R.V., Smith, A.L., Roobol, M.J., 1980. Destruction of St. Pierre, Martinique, by ash-cloud surges,  
1118 May 8 and 20, 1902. *Geology* 8, 472–476. [https://doi.org/10.1130/0091-](https://doi.org/10.1130/0091-7613(1980)8<472:DOSPMB>2.0.CO;2)  
1119 [7613\(1980\)8<472:DOSPMB>2.0.CO;2](https://doi.org/10.1130/0091-7613(1980)8<472:DOSPMB>2.0.CO;2)
- 1120 Flynn, I.T.W., Ramsey, M.S., 2020. Pyroclastic Density Current Hazard Assessment and Modeling  
1121 Uncertainties for Fuego Volcano, Guatemala. *Remote Sensing* 12, 2790.  
1122 <https://doi.org/10.3390/rs12172790>
- 1123 Fujii, T., Nakada, S., 1999. The 15 September 1991 pyroclastic flows at Unzen Volcano (Japan): a flow  
1124 model for associated ash-cloud surges 14.
- 1125 Gertisser, R., Cassidy, N.J., Charbonnier, S.J., Nuzzo, L., Preece, K., 2012. Overbank block-and-ash flow  
1126 deposits and the impact of valley-derived, unconfined flows on populated areas at Merapi  
1127 volcano, Java, Indonesia. *Nat Hazards* 60, 623–648. [https://doi.org/10.1007/s11069-011-](https://doi.org/10.1007/s11069-011-0044-x)  
1128 [0044-x](https://doi.org/10.1007/s11069-011-0044-x)

- 1129 Gueugneau, V., Kelfoun, K., Charbonnier, S., Germa, A., Carazzo, G., 2020. Dynamics and Impacts of the  
1130 May 8th, 1902 Pyroclastic Current at Mount Pelée (Martinique): New Insights From Numerical  
1131 Modeling. *Front. Earth Sci.* 8. <https://doi.org/10.3389/feart.2020.00279>
- 1132 Hovey, E.O., 1904. The 1902-1903 Eruptions of Mont Pelé, Martinique and the Soufrière, St. Vincent.  
1133 Brothers Hollinek.
- 1134 Jenkins, S., Komorowski, J.-C., Baxter, P.J., Spence, R., Picquout, A., Lavigne, F., Surono, 2013. The  
1135 Merapi 2010 eruption: An interdisciplinary impact assessment methodology for studying  
1136 pyroclastic density current dynamics. *Journal of Volcanology and Geothermal Research* 261,  
1137 316–329. <https://doi.org/10.1016/j.jvolgeores.2013.02.012>
- 1138 Jenkins, S.F., Komorowski, J.-C., Baxter, P.J., Charbonnier, S.J., Cholik, N., Surono, 2016. The  
1139 Devastating Impact of the 2010 Eruption of Merapi Volcano, Indonesia, in: Duarte, J.C.,  
1140 Schellart, W.P. (Eds.), *Geophysical Monograph Series*. John Wiley & Sons, Inc., Hoboken, NJ, USA,  
1141 pp. 259–269. <https://doi.org/10.1002/9781119054146.ch12>
- 1142 Kelfoun, K., Gueugneau, V., Komorowski, J.-C., Aisyah, N., Cholik, N., Merciecca, C., 2017. Simulation of  
1143 block-and-ash flows and ash-cloud surges of the 2010 eruption of Merapi volcano with a two-  
1144 layer model. *Journal of Geophysical Research: Solid Earth* 122, 4277–4292.  
1145 <https://doi.org/10.1002/2017JB013981>
- 1146 Kelfoun, K., Legros, F., Gourgaud, A., 2000. A statistical study of trees damaged by the 22 November  
1147 1994 eruption of Merapi volcano (Java, Indonesia): relationships between ash-cloud surges  
1148 and block-and-ash flows. *Journal of Volcanology and Geothermal Research* 100, 379–393.  
1149 [https://doi.org/10.1016/S0377-0273\(00\)00147-5](https://doi.org/10.1016/S0377-0273(00)00147-5)
- 1150 Komorowski, J.-C., Jenkins, S., Baxter, P.J., Picquout, A., Lavigne, F., Charbonnier, S., Gertisser, R.,  
1151 Preece, K., Cholik, N., Budi-Santoso, A., Surono, 2013. Paroxysmal dome explosion during the  
1152 Merapi 2010 eruption: Processes and facies relationships of associated high-energy pyroclastic  
1153 density currents. *Journal of Volcanology and Geothermal Research* 261, 260–294.  
1154 <https://doi.org/10.1016/j.jvolgeores.2013.01.007>
- 1155 Lacroix, A., 1904. *La Montagne Pelee et ses eruptions*. Masson.

- 1156 Lavigne, F., Komorowski, J.-C., Jenkins, S., Baxter, P., Vidal, C., Mei, E.T.W., Picquout, A., Grancher, D.,  
1157 Brunstein, D., N. C., 2011. Satellite Remote-sensing and Field Analysis of Casualties and Damage  
1158 Caused by the 2010 eruption of Merapi Volcano Indonesia. Remote Sensing, natural hazards  
1159 and environmental change, Singapore.
- 1160 Loughlin, S.C., Baxter, P.J., Aspinall, W.P., Darroux, B., Harford, C.L., Miller, A.D., 2002a. Eyewitness  
1161 accounts of the 25 June 1997 pyroclastic flows and surges at Soufrière Hills Volcano,  
1162 Montserrat, and implications for disaster mitigation. Geological Society, London, Memoirs 21,  
1163 211–230. <https://doi.org/10.1144/GSL.MEM.2002.021.01.10>
- 1164 Loughlin, S.C., Calder, E.S., Clarke, A., Cole, P.D., Lockett, R., Mangan, M.T., Pyle, D.M., Sparks, R.S.J.,  
1165 Voight, B., Watts, R.B., 2002b. Pyroclastic flows and surges generated by the 25 June 1997 dome  
1166 collapse, Soufrière Hills Volcano, Montserrat. Geological Society, London, Memoirs 21, 191–  
1167 209. <https://doi.org/10.1144/GSL.MEM.2002.021.01.09>
- 1168 Lube, G., Breard, E.C.P., Cronin, S.J., Jones, J., 2015. Synthesizing large-scale pyroclastic flows:  
1169 Experimental design, scaling, and first results from PELE. Journal of Geophysical Research:  
1170 Solid Earth 120, 1487–1502. <https://doi.org/10.1002/2014JB011666>
- 1171 Lube, G., Breard, E.C.P., Esposti-Ongaro, T., Dufek, J., Brand, B., 2020. Multiphase flow behaviour and  
1172 hazard prediction of pyroclastic density currents. Nature Reviews Earth & Environment 1,  
1173 348–365. <https://doi.org/10.1038/s43017-020-0064-8>
- 1174 Macorps, E., Charbonnier, S.J., Varley, N.R., Capra, L., Atlas, Z., Cabré, J., 2018. Stratigraphy,  
1175 sedimentology and inferred flow dynamics from the July 2015 block-and-ash flow deposits at  
1176 Volcán de Colima, Mexico. Journal of Volcanology and Geothermal Research 349, 99–116.  
1177 <https://doi.org/10.1016/j.jvolgeores.2017.09.025>
- 1178 Mastrolorenzo, G., Petrone, P., Pappalardo, L., Guarino, F.M., 2010. Lethal Thermal Impact at  
1179 Periphery of Pyroclastic Surges: Evidences at Pompeii. PLOS ONE 5, e11127.  
1180 <https://doi.org/10.1371/journal.pone.0011127>
- 1181 Miyahara, T., Endo, K., Tohno, I., Chiba, T., Iso, N., Senda, K., Shinkawa, K., Yasui, M., Komori, J., Ohno,  
1182 M., 1992. Eruptive products of the 1991 Unzen-Hugendake eruption (1). Proc. Inst. Nat. Sci. 27,  
1183 71–80.

- 1184 Moore, J.G., Melson, W.G., 1969. Nuées Ardentes of the 1968 Eruption of Mayon Volcano, Philippines.  
1185 Bull Volcanol 33, 600–620. <https://doi.org/10.1007/BF02596528>
- 1186 Naismith, A., Armijos, M.T., Escobar, E.A.B., Chigna, W., Watson, I.M., 2020. Fireside tales:  
1187 understanding experiences of previous eruptions and factors influencing the decision to  
1188 evacuate from activity of Volcán de Fuego. Volcanica 3, 205–226.  
1189 <https://doi.org/10.30909/vol.03.02.205226>
- 1190 Naismith, A.K., Matthew Watson, I., Escobar-Wolf, R., Chigna, G., Thomas, H., Coppola, D., Chun, C.,  
1191 2019. Eruption frequency patterns through time for the current (1999–2018) activity cycle at  
1192 Volcán de Fuego derived from remote sensing data: Evidence for an accelerating cycle of  
1193 explosive paroxysms and potential implications of eruptive activity. Journal of Volcanology and  
1194 Geothermal Research 371, 206–219. <https://doi.org/10.1016/j.jvolgeores.2019.01.001>
- 1195 Nakada, S., Fujii, T., 1993. Preliminary report on the activity at Unzen Volcano (Japan), November  
1196 1990–November 1991: Dacite lava domes and pyroclastic flows. Journal of Volcanology and  
1197 Geothermal Research 54, 319–333. [https://doi.org/10.1016/0377-0273\(93\)90070-8](https://doi.org/10.1016/0377-0273(93)90070-8)
- 1198 Neri, A., Esposti Ongaro, T., Voight, B., Widiwijayanti, C., 2015. Pyroclastic Density Current Hazards  
1199 and Risk, in: Volcanic Hazards, Risks and Disasters. pp. 109–140.  
1200 <https://doi.org/10.1016/B978-0-12-396453-3.00005-8>
- 1201 Neri, A., Ongaro, T.E., Macedonio, G., Gidaspow, D., 2003. Multiparticle simulation of collapsing  
1202 volcanic columns and pyroclastic flow. Journal of Geophysical Research: Solid Earth 108.  
1203 <https://doi.org/10.1029/2001JB000508>
- 1204 Pallister, J.S., Schneider, D.J., Griswold, J.P., Keeler, R.H., Burton, W.C., Noyles, C., Newhall, C.G.,  
1205 Ratdomopurbo, A., 2013. Merapi 2010 eruption—Chronology and extrusion rates monitored  
1206 with satellite radar and used in eruption forecasting. Journal of Volcanology and Geothermal  
1207 Research, Merapi eruption 261, 144–152. <https://doi.org/10.1016/j.jvolgeores.2012.07.012>
- 1208 Pardini, F., Queißer, M., Naismith, A., Watson, I.M., Clarisse, L., Burton, M.R., 2019. Initial constraints  
1209 on triggering mechanisms of the eruption of Fuego volcano (Guatemala) from 3 June 2018  
1210 using IASI satellite data. Journal of Volcanology and Geothermal Research 376, 54–61.  
1211 <https://doi.org/10.1016/j.jvolgeores.2019.03.014>

- 1212 Pensa, A., Capra, L., Giordano, G., 2019. Ash clouds temperature estimation. Implication on dilute and  
1213 concentrated PDCs coupling and topography confinement. *Sci Rep* 9, 5657.  
1214 <https://doi.org/10.1038/s41598-019-42035-x>
- 1215 Pensa, A., Capra, L., Giordano, G., Corrado, S., 2018. Emplacement temperature estimation of the 2015  
1216 dome collapse of Volcán de Colima as key proxy for flow dynamics of confined and unconfined  
1217 pyroclastic density currents. *Journal of Volcanology and Geothermal Research* 357, 321–338.  
1218 <https://doi.org/10.1016/j.jvolgeores.2018.05.010>
- 1219 Rosi, M., Principe, C., Vecci, R., 1993. The 1631 Vesuvius eruption. A reconstruction based on  
1220 historical and stratigraphical data. *Journal of Volcanology and Geothermal Research, Mount*  
1221 *Vesuvius* 58, 151–182. [https://doi.org/10.1016/0377-0273\(93\)90106-2](https://doi.org/10.1016/0377-0273(93)90106-2)
- 1222 Sulpizio, R., Dellino, P., 2008. Chapter 2 Sedimentology, Depositional Mechanisms and Pulsating  
1223 Behaviour of Pyroclastic Density Currents, in: Gottsmann, J., Martí, J. (Eds.), *Developments in*  
1224 *Volcanology, Caldera Volcanism: Analysis, Modelling and Response*. Elsevier, pp. 57–96.  
1225 [https://doi.org/10.1016/S1871-644X\(07\)00002-2](https://doi.org/10.1016/S1871-644X(07)00002-2)
- 1226 Suroño, Jousset, P., Pallister, J., Boichu, M., Buongiorno, M.F., Budisantoso, A., Costa, F., Andreastuti, S.,  
1227 Prata, F., Schneider, D., Clarisse, L., Humaida, H., Sumarti, S., Bignami, C., Griswold, J., Carn, S.,  
1228 Oppenheimer, C., Lavigne, F., 2012. The 2010 explosive eruption of Java’s Merapi volcano—A  
1229 ‘100-year’ event. *Journal of Volcanology and Geothermal Research* 241–242, 121–135.  
1230 <https://doi.org/10.1016/j.jvolgeores.2012.06.018>
- 1231 Trolese, M., Giordano, G., Komorowski, J.-C., Jenkins, S.F., Baxter, P.J., Cholikh, N., Raditya, P., Corrado,  
1232 S., 2018. Very rapid cooling of the energetic pyroclastic density currents associated with the 5  
1233 November 2010 Merapi eruption (Indonesia). *Journal of Volcanology and Geothermal*  
1234 *Research* 358, 1–12. <https://doi.org/10.1016/j.jvolgeores.2018.06.004>
- 1235 Valentine, G.A., 1998. Damage to structures by pyroclastic flows and surges, inferred from nuclear  
1236 weapons effects. *J Volcanol Geotherm Res* 87, 117–140.
- 1237 Valentine, G.A., Wohletz, K.H., 1989. Numerical models of Plinian eruption columns and pyroclastic  
1238 flows. *Journal of Geophysical Research: Solid Earth* 94, 1867–1887.  
1239 <https://doi.org/10.1029/JB094iB02p01867>

- 1240 Voight, B., Constantine, E.K., Siswamidjono, S., Torley, R., 2000. Historical eruptions of Merapi  
1241 Volcano, Central Java, Indonesia, 1768–1998. *Journal of Volcanology and Geothermal Research*  
1242 100, 69–138. [https://doi.org/10.1016/S0377-0273\(00\)00134-7](https://doi.org/10.1016/S0377-0273(00)00134-7)
- 1243 Voight, B., Davis, M.J., 2000. Emplacement temperatures of the November 22, 1994 nuée ardente  
1244 deposits, Merapi Volcano, Java. *Journal of Volcanology and Geothermal Research* 100, 371–377.  
1245 [https://doi.org/10.1016/S0377-0273\(00\)00146-3](https://doi.org/10.1016/S0377-0273(00)00146-3)
- 1246 White, N., 2018. Shocking satellite photos show entire towns obliterated after Guatemala’s “Volcano  
1247 of Fire” buried them in tons of ash that crushed hundreds of homes and burned 300 people  
1248 alive. Mail Online.
- 1249 Wibowo, H.E., Purnama Edra, A., Harijoko, A., Anggara, F., 2018. Emplacement Temperature of the  
1250 Overbank and Dilute-Detached Pyroclastic Density Currents of Merapi 5 November 2010  
1251 Events using Reflectance Analysis of Associated Charcoal. *J. Appl. Geol.* 3, 41.  
1252 <https://doi.org/10.22146/jag.42445>
- 1253 World Bank, 2018. June 3, 2018 Volcán de Fuego Guatemala Eruption Global Rapid Post Disaster  
1254 Damage Estimation Grade Report (Global Rapid Post Disaster Damage Estimation (GRADE)  
1255 Report No. AUS000903).
- 1256 Yamamoto, T., Takarada, S., Suto, S., 1993. Pyroclastic flows from the 1991 eruption of Unzen volcano,  
1257 Japan. *Bull Volcanol* 55, 166–175. <https://doi.org/10.1007/BF00301514>
- 1258